

# **In-situ hydrogenolysis of glycerol using hydrogen produced via aqueous phase reforming of glycerol over sonochemically synthesized Nickel based nano-catalyst**

Ain Syuhada<sup>b</sup>, Mariam Ameen<sup>a,b,\*</sup>, Mohammad Tazli Azizan<sup>d</sup>, Aqsha Aqsha<sup>e\*</sup>, Mohd Hizami Mohd Yusoff<sup>a,b</sup>, Anita Ramli<sup>a,c</sup>, Mohamad Sahban Alnarabiji<sup>b</sup> and Farooq Sher<sup>f</sup>

<sup>a</sup>*HiCoE, Center for Biofuel and Biochemical Research (CBBR), Institute of Sustainable Buildings (ISB), Universiti Teknologi PETRONAS, 32610, Seri Iskandar, Perak, Malaysia*

<sup>b</sup>*Department of Chemical Engineering, Universiti Teknologi PETRONAS, 32610, Seri Iskandar, Perak, Malaysia*

<sup>c</sup>*Department of Fundamental and Applied Science, Universiti Teknologi PETRONAS, 32610, Seri Iskandar, Perak, Malaysia*

<sup>d</sup>*Faculty of Chemical Engineering Technology, Universiti Malaysia Perlis, 01000 Kangar, Perlis*

<sup>e</sup>*Department of Bioenergy and Chemurgy, Faculty of Technology Industry, Institut Teknologi Bandung, Indonesia*

<sup>f</sup>*School of Mechanical, Aerospace and Automotive Engineering, Faculty of Engineering, Environmental and Computing, Coventry University, Coventry, CV1 5FB, United Kingdom*

## **\*Corresponding author:**

E-mail address: E-mail: [mariam.ameenkk@utp.edu.my](mailto:mariam.ameenkk@utp.edu.my); (M. Ameen), [aqsha@che.itb.ac.id](mailto:aqsha@che.itb.ac.id) (A. Aqsha)

## Abstract

1,3-Propanediol (1,3-PDO) is a commercially valuable chemical for the production of polytrimethylene terephthalate polymers and polyurethane. In this study, the production of 1,3-PDO was investigated via aqueous phase reforming (APR) and selective hydrogenolysis of glycerol over Ni-Ca/CeO<sub>2</sub> catalysts synthesized by sonochemical (Us) and wet impregnation (WI) methods. The experiments were performed in a batch reactor at 20 bar, 230 °C and 450 rpm for 1 h. The synthesized catalysts were characterized using XRD, TEM, FESEM, BET, H<sub>2</sub>-TPR, XPS, CO-chemisorption and NH<sub>3</sub>-TPD to offer a deeper understanding of the physio-chemical and surface characteristics. The results revealed that sonochemical catalysts showed a larger surface area, smaller crystallite size, low reduction temperature and more homogenous particles distribution compared to wet impregnation catalysts. For both preparation methods, monometallic Ni/CeO<sub>2</sub> catalysts showed the highest activity, whereas Ca modification of Ni/CeO<sub>2</sub> catalysts significantly decreased the activity of the catalysts. The highest yield and selectivity of 1,3-PDO were found to be 19.54% and 42.73%, respectively using Ni/CeO<sub>2</sub>\_Us catalyst. The best catalyst was further utilized for parameters optimization study to observe the effect of varying glycerol concentration (10 to 25 vol.%), temperature (210 to 250°C) and pressure (10 to 30 bar) on the yield and selectivity of 1,3-PDO and glycerol conversion. The results demonstrated that the highest yield (19.54%) and selectivity (42.73%) of 1,3-PDO were obtained over 10 vol.%, 230 °C and 20 bar with glycerol conversion of 54.26%. This present study provides a promising and economical process of converting glycerol to 1,3-PDO which is suitable for application in industry.

**Keywords:** Renewable fuels; Aqueous phase reforming; hydrogenolysis; glycerol; 1,3-Propanediol; sonochemically synthesized catalyst and Ni/CeO<sub>2</sub> catalyst.

## 1 Introduction

Production of 1,3-propanediol(1,3-PDO) from glycerol has become a great interest as it is a highly expensive value-added chemical used in the production of polytrimethylene terephthalate (PTT) polymer and polyurethane [1]. Currently, 1,3-PDO is produced through hydrogenolysis of glycerol utilizing active metal catalysts such as platinum (Pt) [2, 3], copper (Cu) [4] and nickel (Ni) [5]. However, the consumption of hydrogen gas during the hydrogenolysis reaction cause the process to be less cost-effective and highly risks as it may lead to explosion if there is leakage [6]. Therefore, to fully eliminate the usage of hydrogen gas in the hydrogenolysis process, the combination of APR with selective hydrogenolysis reaction was identified as the best alternative method.

APR process was introduced in 2002 by Dumesic's group [7]. The APR process is carried out at relatively low temperature (200–250 °C) and high pressure (1.5 MPa- 5.0 MPa) which assists to reduce the undesirable decomposition reaction [8]. This process also favours water gas shift (WGS) reaction that produces hydrogen which could be further used for hydrogenolysis reaction to produce various gaseous and liquid products[9]. A few number of works have investigated the possibility of combining APR and hydrogenolysis of glycerol using Pt catalysts [7, 10-12], Cu-Zn/Al catalyst [13] and Ni/Al-Fe catalyst [14]. Liu, Tamura [15] investigated on the production of propylene glycol through combined APR and hydrogenolysis of glycerol over IrReO<sub>x</sub>/SiO<sub>2</sub> catalyst in an autoclave reactor. They reported that, the highest 1,3-PDO selectivity of up to 9.6 % with 20% glycerol conversion were obtained.

More attention has been made on the development of suitable catalyst for the 1,3-PDO production using noble or transition metal catalysts (Pt, Ru, Ir, Re and Ni) alone or promoted with other metal oxide or salts (Ca, Mo and Cu) supported on various supports ( $\text{CeO}_2$ ,  $\text{WO}_3$  and  $\text{Al}_2\text{O}_3$ ) [4, 16, 17]. A Bronsted acid catalyst is necessary for the reaction to proceed via glycerol dehydration to 3-HPA then followed by in-situ hydrogenolysis of 3-HPA to 1,3-PDO [18, 19]. Among these catalysts, Ni has developing much interest for glycerol hydrogenolysis as it is highly selective towards C-O bond cleavage [20]. Meanwhile for the selection of promoter, Ca promoter is selected for this study as it has shown promising performance during hydrogenolysis reaction as well significantly improved the particles distribution [21]. Gong, Zhao [22] also agreed that the doping of Ca on the  $\text{Co}_2\text{-Al}_3$  catalyst significantly increase the yield of 1,2-propanediol produced via hydrogenolysis of glycerol which shows that this catalysts is highly selective for hydrogenation reaction.

The  $\text{CeO}_2$  was selected as the catalyst support for this application due to its promising performance in improving the metal dispersion and metal-support interaction [23]. Therefore, these factors have a good impact on the catalytic activity of nickel supported catalysts in the reforming of hydrocarbons [24]. Bastan, Kazemeini [25] studied the effect of varying the composition of cerium on the catalytic activity of  $\text{Ni/Ce}_x\text{Zr}_{1-x}\text{O}$  catalyst in APR of glycerol. It was found that the ceria itself has a great influence on the catalyst activity and stability during the reaction.

The efficiency of the catalysts was also affected by the catalyst preparation method. It was reported that, the conventionally synthesized catalyst commonly using impregnation method are

highly agglomerate due to uneven distribution of the metal on the support [25]. Therefore, extensive development on catalyst synthesizing method has been made by introducing ultrasound irradiation. This method has been proven to improve the physicochemical properties of the catalysts due to cavitation phenomena which involved the formation and collapse of micro bubbled in a split second [26]. Ahmadi, Haghighi [27] agreed that sonochemically synthesized catalyst possesses a smaller particle size and a more homogeneous distribution of metals on the support. .

To the best of our knowledge, the combined APR and selective hydrogenolysis of glycerol for 1,3-PDO production using active metals catalysts supported on CeO<sub>2</sub> using the sonochemical approach have not been reported previously, which is the novelty of the present work. The purpose of using APR reaction exclusively to produce 1,3-PDO is aimed to utilize the in-situ hydrogen produce during APR reaction to convert the glycerol to 1,3-PDO via hydrogenolysis reaction. In the present study, the APR and selective hydrogenolysis of glycerol are carried out in a batch reactor over a series of Ca doped Ni-based catalysts supported on CeO<sub>2</sub>. The performance of the catalysts during the reaction are investigated based on the yield and selectivity of 1,3-PDO and glycerol conversion.

## **2 Experimental**

### **2.1 Materials**

Nickel nitrate hexahydrate (Ni(NO<sub>3</sub>)<sub>2</sub>·6H<sub>2</sub>O), calcium chloride dihydrate (CaCl<sub>2</sub>·2H<sub>2</sub>O) cerium dioxide (CeO<sub>2</sub>), glycerol and 1,3-Propanediol(99.99%) standard were all purchased from Merck Company, Malaysia. All the chemicals used were of analytical grade and used without any

further purification. Purified hydrogen (99.99%) and nitrogen (99.99%) gases were supplied by Linde Malaysia.

## 2.2 Catalyst preparation

The Ni-xCa/CeO<sub>2</sub> (where x=0, 0.5, 3 and 5) catalysts were synthesized using a typical sonochemical (Us) [28] and wet impregnation (WI) [29] methods. The Ni(NO<sub>3</sub>)<sub>2</sub>·6H<sub>2</sub>O and CaCl<sub>2</sub>·2H<sub>2</sub>O salts which were used as Ni and Ca precursor, respectively were dissolved separately in deionized water according to the catalyst formulation. Then, the aqueous solutions of the salts were doped simultaneously onto the support. For the sonochemical method, the mixture was sonicated using ultrasound sonicator (Model: Q700 Sonica; Fisher Scientific) at 90 W for 45 min with 30 s pulse ON and 5 s OFF. Whereas, for the wet impregnation method, the mixture was stirred at room temperature for 4 h and 350 rpm. The samples were then dried using vacuum oven at 110 °C for 24 h and calcined using a box furnace at 500 °C for 4 h in the static air environment. The synthesized catalysts were denoted as Ni-xCa/CeO<sub>2</sub>\_Us and Ni-xCa/CeO<sub>2</sub>\_WI (where; x=0, 0.5,3 and 5).

## 2.3 Characterization of catalysts

X-Ray Diffraction (XRD) analysis was performed by using X' Pert 3 Powder & Empyrean, PANalytical diffractometer equipped with Cu K $\alpha$  radiation source ( $\lambda=1.5406\text{\AA}$ ) operating at 45kV and 40Ma [14]. The diffraction data were collected in the  $2\theta$  range of  $10^\circ$ - $70^\circ$  in continuous mode. The crystallite size of the catalysts was determined using Scherrer equation [4];  $D=K\lambda/(\beta\cos \theta)$  where  $D$  = crystallite size,  $K$  = crystalline shape factor (0.9),  $\lambda = 0.154\text{nm}$ ,  $\beta$  = line broadening at half the maximum intensity (in radians) and  $\theta$  = peak angle (in radians). The textural properties of the catalysts were determined from nitrogen adsorption-desorption measurement using micromeritics ASAP 2020 instrument. The specific surface area was

calculated using BET analysis [4] and the pore volume size were determined using BJH method [30].

The Field Emission Scanning Electron Microscope (FESEM) analysis was performed by using VPFESEM, Zeiss Supra 55VP operating at 5 kV. This FESEM analysis was performed together with Electron Dispersive X-ray(EDX) and dot mapping analysis. Temperature programmed reduction (H<sub>2</sub>-TPR), temperature-programmed desorption (NH<sub>3</sub>-TPD) and CO-chemisorption analysis were performed using TPDRO, Model:1100, Thermo Scientific equipped with thermal conductivity detector (TCD). For the TPR analysis, 10 g of catalysts powder were firstly degassed inflow of nitrogen (N<sub>2</sub>) gas at 300 °C for 1.5 hours to remove all the moisture. Then, the catalysts were cooled down to 25 °C by N<sub>2</sub> stream and heated until 950 °C at the rate of 10 °C/min in the presence of 5% H<sub>2</sub> in Ni with holding time of 10 min [14]. Meanwhile, for the TPD analysis, 25 mg of catalysts powder were first pretreated under helium (He) gas with a flow of 80 mL/min at 300 °C for 1 h. Then, the catalysts were cooled down to 25 °C and 50 mL/min of 10 vol% NH<sub>3</sub> in He gas were injected into the catalysts to ensure all the catalysts are saturated with NH<sub>3</sub>. The catalyst bed was heated to 800 °C at a heating rate of 30 °C/min [31]. Meanwhile, the CO-chemisorption analysis was carried out at 30 °C with a successive injection of 0.5 mL CO samples via calibrated loop into the 30 mL/min He carrier until a saturated peak was observed to measure the CO uptake [32]. Transmission Electron Microscopy (TEM) micrographs were obtained using an electron microscope (Model: Zeiss Libra 200 made in the USA) with accelerating voltage of 100–200 kV. The average diameter of the metal particles was analyzed using Image J software. X-ray Photoelectron Spectroscopy (XPS) analysis was carried out using utilizing K-Alpha instrument equipped with monochromatic Al K $\alpha$  source (h $\nu$ =1486.6

eV) operating at 150 W, a double-sided adhesive tape vessel and detector at the pressure of  $1 \times 10^{-9}$  Torr. The spectra were recorded at narrow scan and survey spectra of 40 eV and 160 eV respectively.

## 2.4 Experimental setup

The activity tests were carried out in PREMEX Autoclave High-Pressure batch reactor equipped with a magnetic stirrer, thermocouple and two input valves for gas inserting and releasing (Fig. 1). The catalysts were first reduced under  $H_2$  flow 50 mL for 1 h at their respective reduction temperature determined from  $H_2$ -TPR analysis [33]. After the reduction process, pure  $N_2$  gas was purged into the reactor to remove the traces of hydrogen left on the catalysts. The reactor was let to cool down to 100 °C and Glycerol solution (10 vol.%) was put into the reactor and sealed. The reaction was conducted at 230 °C, 20 bar of purified nitrogen and 450 rpm for 1 h with and without catalyst as blank run to observe the presence of in-situ hydrogen produced during the reaction which was confirmed with GC-TCD [33]. Later, all the catalysts were screened at similar reaction condition. The liquid products were analyzed using High-Performance Liquid Chromatography (HPLC) equipped with a refractive index (RI) detector. The analysis was performed using Eclipse XDB C18 column (5  $\mu$ m, 46 $\times$ 150 mm) with total runtime of 35 min and 0.005 M sulfuric acid as mobile phase was injected at a flow rate of 0.6 mL/min into the system [30]. The yield [5] and selectivity of 1,3-PDO [1] and glycerol conversion [34] were determined using the Eq. (1) to Eq. (3).

$$\text{Yield of 1,3 - PDO} = \frac{\text{Mass of 1,3-PDO produced}}{\text{Total mass of product produced}} \times 100\% \quad (1)$$

$$\text{Selectivity OF 1,3 - PDO} = \frac{\text{Mass of 1,3-PDO produced}}{\text{Total mass of glycerol consumed}} \times 100\% \quad (2)$$

$$\text{Conversion of glycerol} = \frac{\text{Mass of glycerol consumed}}{\text{Mass of glycerol in}} \times 100\% \quad (3)$$

## 2.5 Parameters optimization

The best catalyst was further utilized for parameters optimization study to observe the effect of varying glycerol to catalyst weight ratio ( $W_{\text{glycerol}}/W_{\text{catalyst}}$ ), temperature and pressure on yield and selectivity of 1,3-PDO and glycerol conversion. The range of the parameters used in this optimization study was selected based on the work conducted by Remón, Giménez [35] and also considering the reactor limitation. The agreed range of parameters for this study are as follow:  $W_{\text{glycerol}}/W_{\text{catalyst}} = 3.15$  to  $15.77$   $g_{\text{glycerol}}/g_{\text{catalyst}}$ , temperature = 210 to 250 °C and pressure =10 to 30 bar. Meanwhile, the other parameters such as reaction time and stirring rate were kept constant at 1 h and 450 rpm, respectively. The reaction products were analyzed using HPLC analysis as mentioned in Section 2.4. The yield and selectivity of 1,3-PDO and glycerol conversion were determined using Eq. (1) to Eq. (3).

## 3 Results and discussion

### 3.1 Physicochemical properties of catalysts

The XRD patterns of CeO<sub>2</sub> support and all the synthesized catalysts are shown in Fig. 2. Detailed analysis on the XRD patterns showed that the CeO<sub>2</sub> peaks were observed at  $2\theta=28.54^\circ$ ,  $33.08^\circ$ ,  $47.48^\circ$ ,  $56.49^\circ$ ,  $59.09^\circ$ ,  $69.62^\circ$ ,  $76.92^\circ$ ,  $79.26^\circ$  and  $88.71^\circ$  (JCPDS No. 34-0394) which represents the cubic structure of CeO<sub>2</sub> [36]. Whereas the diffraction peaks of the cubic structure of NiO are observed at  $2\theta=37.3^\circ$ ,  $37.49^\circ$ ,  $43.1^\circ$  and  $62.93^\circ$  (JCPDS No.47-1049) [28, 33]. The diffraction peaks of CaO are observed at  $2\theta= 37.32^\circ$  and  $54.1^\circ$  (JCPDS NO. No. 82-1691) which represents cubic structure [21].

The inset of the XRD patterns of both sonochemical and wet impregnation catalysts revealed that the main peaks of the catalysts shifted towards the smaller angle and smaller line broadening with an increased in the Ca doping. This shift in peaks and smaller line broadening of the catalysts increase the crystallite size . Rajivgandhi, Ramachandran [37] also reported that the shift in peak position and line broadening of the planes significantly affect the crystallite size of the compound.

Table 1 shows the average crystallite size of NiO, CaO and CeO<sub>2</sub> crystals of each catalyst samples calculated using the Scherer equation. From the results, it is observed that the increased in the amount of Ca doping from 0 to 5 wt.% on the Ni/CeO<sub>2</sub> catalysts synthesized by sonochemical significantly increase the crystallite size of NiO, CaO and CeO<sub>2</sub> crystals from 2.10 to 2.44 nm, 2.03 to 2.07 nm and 2.78 to 2.97 nm, respectively.

Meanwhile for catalysts synthesized by wet impregnation methods, the increase in Ca doping from 0 to 5 wt.%, significantly increased the crystallite size of NiO, CaO and CeO<sub>2</sub> crystals from 2.27 to 2.60 nm, 2.10 to 2.30 nm and 2.80 to 3.05 nm, respectively. This indicates that the increased in metal doping leads to an increase in particles agglomeration due to the uneven distribution of the metals over the support. Comparatively, the result also shows that sonochemical catalysts have a slightly smaller crystallite size compare to WI catalysts. Therefore, it can be proved that the high power of ultrasound irradiation promotes more homogeneous particles distribution which significantly affects the crystallite size of the catalysts. The catalyst with the smallest crystallite size is predicted to be the most active during the catalytic reaction as it prepares a larger surface area and more active sites for the reaction to

occur[26]. These findings also agreed with Rahbar Shamskar, Meshkani [38] which also reported that the ultrasound irradiation improved the distribution of the particles and decreased the agglomeration of the particles which resulted in smaller crystallite size of NiO-Al<sub>2</sub>O<sub>3</sub> catalysts.

The specific surface area (SSA), pore volume and pore size of the synthesized catalysts are shown in Table 1. From the results, it is observed that the surface area of the catalysts for both methods decreased with increased metal loading [39]. This decrease in surface area at higher metal loading is due to larger particles size effected by particles agglomeration [39]. A comparison of sonochemical and wet impregnation catalysts shows that sonochemical catalysts have a slightly bigger surface area. This is mainly caused by ultrasound irradiation which helps to reduce particles agglomeration by promoting homogeneous metals distribution. The catalyst with a larger surface area is believed to be more active during the catalytic reaction as it has more active sites for the reaction to occur [38]. These results are in line with the XRD analysis shown in Fig. 2, confirming that smaller particles size results in higher SSA.

The pore volume and pore size are also affected by the ultrasound irradiation. The results revealed that the pore volume and pore size of catalysts decreased with an increase in metal loading. The results also show that sonochemical catalysts have a bigger pore volume and pore size compared to wet impregnation catalyst. Higher pore volume and pore size of sonochemical catalysts are caused by cavitation phenomena that promote homogeneous metals distribution [28]. However, the lower pore volume and pore size of wet impregnation catalyst confirmed that there is blockage of pores by loaded metals. Xu, Yang [31] observed that the increased in Ca

compositions, decreased the surface area and pore volume which caused by particles agglomeration due to uneven metal particles distribution (Table 1).

The N<sub>2</sub> adsorption-desorption isotherms of sonochemical and wet impregnation catalysts is shown in Fig. 3(a) and (b) respectively. It is observed that the isotherms of all the synthesized catalysts are similar to type IV isotherm which indicate that the catalysts are in mesoporous structure with particle diameter between 2 to 50 nm [40, 41]. The FESEM images, EDX spectra and dot mapping images of the synthesized catalysts are shown in Fig. 4. From the FESEM images it is observed that at high metal loadings, the catalysts might experience particles agglomeration due to the uneven distribution of metals on the support. This finding is supported by the EDX spectra and dot mapping images which also proved that at high metals loading the catalysts are highly agglomerate. This particles agglomeration may lead to catalysts deactivation during the reaction. He, Yao [42] also agreed that at high metal loadings, the catalysts experienced serious particles agglomeration due to non-homogeneous particles distribution. This is supported by the crystallite size (Table 1) calculated from XRD analysis which shows that the average crystallite size of NiO, CaO and CeO<sub>2</sub> crystals increased with an increase in the amount of metals loading.

Besides that, SSA determined from the BET method shows that the SSA of the catalysts decreased with increased metals loadings (Table 1). Comparatively, the FESEM images, EDX spectra and dot-mapping images of sonochemical and wet impregnation catalysts show that the metal particles of sonochemical catalysts are homogeneously distributed on the support (Fig. 4). Meanwhile, for wet impregnation catalysts, particles agglomeration is observed at a particular area which might be caused by the uneven distribution of metals. Therefore, this confirmed that

the ultrasound irradiation significantly reduced the particle agglomeration by promoting homogeneous metals distribution [38, 43]. These results are supported by the crystallite size and SSA determined from XRD and BET analysis respectively (Table 1). The H<sub>2</sub>-TPR analysis was conducted to determine the reducibility and interaction between metal and support of sonochemical and wet impregnation catalysts. Fig. 5 represents the individual reduction profile of all the synthesized catalysts.

It is observed that for all the catalysts, one broad peak is present in the range of 300-500 °C. The peak of Ni/CeO<sub>2</sub>\_WI, Ni-0.5Ca/CeO<sub>2</sub>\_WI, Ni-3Ca/CeO<sub>2</sub>\_WI and Ni-5Ca/CeO<sub>2</sub>\_WI catalysts are observed at 392, 402, 406 and 420 °C respectively. Whereas the peak of Ni/CeO<sub>2</sub>\_Us, Ni-0.5Ca/CeO<sub>2</sub>\_Us, Ni-3%Ca/CeO<sub>2</sub>\_Us and Ni-5Ca/CeO<sub>2</sub>\_Us catalysts are observed at 352, 372, 378 and 402 °C respectively. These peaks represent the reduction of weakly interacted NiO to Ni [38, 44]. The reduction profiles of the catalysts show that the increased in metals loading shifted the TPR peaks towards higher temperature for both preparation methods. This indicated the increased in Ca loading decreased the reducibility of the catalysts due to stronger interaction between metals and support [21]. This is mainly caused by the agglomeration of particles and non-homogeneous particles distribution at higher metals loading.

Besides that, particles size also has a great influence on the reducibility of the catalysts. Catalysts with smaller particles size are reduced at slightly low temperature due to weak interaction between metals and support[39]. This is the reason why the increased in metal loading leads to an increase in catalysts reducibility due to an increase in particles size. This finding agreed with the FESEM, XRD and BET analysis which proved that at low metals loading, the metals are

more homogeneously distributed which results in smaller particles size. Comparatively, for sonochemical and wet impregnation catalysts with the same formulation, it is observed that the sonochemical catalyst has a slightly lower reduction temperature (Fig. 5). This is due to homogeneous particles distribution which leads to smaller particles size possess by sonochemical catalysts.

Meanwhile, wet impregnation catalysts show a higher reduction temperature due to non-homogeneous particles distribution which leads to bigger particles size and strong interaction between metals and support [38]. Besides that, it is also observed that sonochemical catalysts have a sharper reduction peak compared to wet impregnation catalyst. This indicates that sonochemical catalysts consumed less hydrogen to breaks the weak interaction between metals and support compared to wet impregnation catalyst. The catalyst with lower reduction temperature has lower binding energy between metal and support as well as lower hydrogen consumption compared to catalyst with higher reduction temperature [39]. As mention above, the catalyst with strong metals-support interactions and smaller particles size results in high dispersion is desirable for this in-situ hydrogenolysis reaction [45]

### **3.2 Catalytic performance and selective hydrogenolysis of glycerol**

The APR and selective hydrogenolysis of glycerol were performed using PREMEX autoclave batch reactor at the following reaction conditions: 230 °C, 20 bar, the reaction time of 1 h, 10 wt.% glycerol and stirring rate of 450 rpm. A blank test of glycerol as reactant was performed at similar reaction conditions without the presence of a catalyst to evaluate the in-situ H<sub>2</sub> produced via APR of glycerol. The blank run exhibited poor H<sub>2</sub> production performance of only 0.1 mol was produced after 1 h of reaction time. Subsequently, a blank test of 10 g of CeO<sub>2</sub> support was

performed at similar reaction conditions. The result showed that the H<sub>2</sub> production slightly improved to 0.2 mol and a smaller yield of 1,3-PDO of approximately 2.05% were found in the gas and liquid products respectively. Therefore, it has anticipated that this in-situ hydrogen produced via APR reaction will be able to facilitate the hydrogenolysis of glycerol to 1,3-PDO. Then, the APR and selective hydrogenolysis of glycerol were performed using all the synthesized catalysts at similar reaction conditions. The catalytic performance of the synthesized catalysts for this APR and selective hydrogenolysis reaction were determined by comparing the yield and selectivity of 1,3-PDO and glycerol conversion to the liquid product as summarized in Fig. 6.

The results obtained revealed that the yield of 1,3-PDO decreases with an increased in the amount of Ca doping for both preparation methods. For Us catalysts, the increased in the amount of Ca doping from 0 to 5 wt.%, decreased the 1,3-PDO yield from 19.54 to 5.36%. Meanwhile, for WI catalysts, the 1,3-PDO yield decreased from 4.08 to 2.15% with an increased in the amount of Ca loading from 0 to 5 wt.%. The results show that, for both preparation methods, monometallic Ni/CeO<sub>2</sub> catalysts give the highest yield of 1,3-PDO. This is mainly caused by the Ni active sites which act as dehydrogenating and hydrogenating catalysts. It is also reported in the literature that Ni alone is more suitable for the hydrogenolysis reaction route [46].

Similarly, for 1,3-PDO selectivity it is also observed that the 1,3-PDO selectivity decreased with an increased in the amount of Ca doping for both preparation methods (Fig. 6). For Us catalysts, the increased in Ca doping from 0 to 5 wt.%, decreased the 1,3-PDO selectivity from 42.73 to 10.39%. Meanwhile, for WI catalysts, the 1,3-PDO selectivity decreased from 7.69 to 3.90% with an increased in the amount of Ca doping from 0 to 5 wt.%. Although it has been reported

in the literature that Ca as a promoter has shown good performance during the hydrogenolysis reaction, however for our study the addition of Ca brings a negative impact on the yield of 1,3-PDO produced via in-situ hydrogenolysis of glycerol. This might be caused by the reduction in the Bronsted acid sites of the catalysts affected by the basic properties Ca [47]. As reported in the literature, Bronsted acid sites are necessary to ensure that the reaction proceeds via dehydration and hydrogenation of glycerol to 1,3-PDO [45].

Besides that, this might also cause by the reduction in the active sites of the catalysts due to particles agglomeration at higher metal loading. The decreased in the amount of H<sub>2</sub> produced during APR reaction could also be the reason for decreased in the 1,3-PDO yield and selectivity with an increased in the amount of Ca doping. This finding is supported by García-Fernández, Gandarias [48] which also reported that the lower availability of H<sub>2</sub> significantly affects the distribution of 1,3-PDO in the product. In the comparison of sonochemical and wet impregnation catalysts with similar composition, the 1,3-PDO yield and selectivity obtained using sonochemical catalysts is slightly higher than the wet impregnation catalysts. This is caused by the ultrasound irradiation that improved the metal dispersion which resulted in a larger surface area and more active sites for the reaction to occur.

For the glycerol conversion to liquid products, it is observed that all the catalysts have approximately 40-60% glycerol conversion except for CeO<sub>2</sub> support (Fig.6). This result is in line with the reported data for this APR and selective hydrogenolysis of glycerol [45]. This high conversion of glycerol to liquid products might be due to operating conditions such as temperature, pressure, glycerol concentration and reaction times. During this reaction, glycerol

was converted into respective liquid products at their vaporized temperature through various processes such as hydration and hydrogenolysis [49]. Similarly, it is also observed that the glycerol conversion of Us and WI catalysts decreased from 54.26 to 48.44% and 46.90 to 37.22% respectively, with an increased in the amount of Ca composition from 0 to 5 wt.%. At higher metals loading, the catalysts are less active due to smaller surface area. In comparison, sonochemical catalysts have higher glycerol conversion compared to wet impregnation catalysts. This is because the particles of sonochemical catalysts are homogeneously distributed which resulted in smaller particles size and higher active sites for the reaction.

Moreover, Table 2 shows the comparison of the different catalysts used and their synthesizing methods as well as different technology used in the production of 1,3-PDO utilizing glycerol. From the table, it can be concluded that this present study, utilized a rather novel catalyst and technology which give significant results in term of 1,3-PDO selectivity when compared with the best results reported on the 1,3-PDO via the conventional method. This study mainly focuses on the effect of varying amount of Ca doping and comparative study of the conventionally synthesized catalyst and sonochemically synthesized catalyst. Overall, Ni/CeO<sub>2</sub>\_Us catalyst was identified as the best catalyst for 1,3-PDO production via APR of glycerol which has the highest yield and selectivity of 1,3-PDO. The best-designed catalyst is further characterized using TEM, NH<sub>3</sub>-TPD, XPS and Co-Chemisorption analysis to compare its physicochemical properties with catalysts synthesized by conventional methods.

The TEM images and particles size distribution of Ni/CeO<sub>2</sub>\_Us and Ni/CeO<sub>2</sub>\_WI catalysts are shown in Fig. 7. From the TEM images, it is observed that catalyst particles have mainly

truncated octahedral morphology. Meanwhile, from the particles size distribution, it is observed that sonochemical catalyst has slightly smaller particles size distribution compared to wet impregnation catalysts. This proved that ultrasound irradiation promotes a more homogeneous particle distribution which resulted with larger surface area and higher catalytic activity for APR and selective C-O hydrogenolysis of glycerol. Meanwhile, wet impregnation catalyst has a slightly larger particle size mainly due to particle agglomeration which reduced the performance of catalysts during the reaction. The maximum particle size of Ni/CeO<sub>2</sub>\_Us and Ni/CeO<sub>2</sub>\_WI catalysts are obtained at 30 nm and 50 nm respectively, while the calculated average particle sizes of Ni/CeO<sub>2</sub>\_Us and Ni/CeO<sub>2</sub>\_WI are 22 nm and 40 nm respectively. This result is in line with the XRD analysis discussed in Section 3.1.

The number of acidic sites and strength of Ni/CeO<sub>2</sub>\_Us and Ni/CeO<sub>2</sub>\_WI catalysts were determined using NH<sub>3</sub>-TPD analysis. Fig. 8 shows the individual desorption profile of the synthesized catalysts. According to [1] the strength of acidic sites of the catalyst is categorized into three peak temperature regions; Region I: 150 -300 °C represent the weak acid site which is also known as Lewis acid, Region II: 300-450 °C represent the moderate acid site and Region III: 450-650 °C represent strong acid site which also known as Bronsted acid. From the desorption profile, it is observed that the number of peaks present in the sonochemical catalyst is higher than the wet impregnation catalyst which indicates that sonochemical catalyst has more acidic sites. Higher surface area and homogeneous dispersion of metals over the support is identified as the main reason why sonochemical catalyst has more acidic sites compared to wet impregnation catalyst which is also agreed by the literature [39].

Besides that, from the desorption profile, it is also observed that both catalysts possess a high amount of Bronsted acid sites due to the present of desorption peak at high temperature between 450-650 °C (Region III). The first desorption peak for both sonochemical and wet impregnation catalysts appeared at 325 °C (Region II) while the second desorption peak appeared at 445°C (Region III). The third desorption peak that appeared at 500°C is observed for both sonochemical and wet impregnation catalysts while the fourth and fifth desorption peaks at 600 °C and 750 °C (Region III) is only observed for the sonochemically synthesized catalyst. Thus, it is observed that sonochemical catalyst poses more active sites and higher desorption of ammonia. The catalyst with stronger acids sites is believed to be more active and selective for in-situ hydrogenolysis of glycerol to 1,3-PDO.

The oxidation states of the Ni/CeO<sub>2</sub>\_Us and Ni/CeO<sub>2</sub>\_WI catalysts were determined using XPS analysis. The fitted XPS spectra of Ni 2p of the synthesized catalysts were showed in Fig. 9(a) and (b) respectively. Detailed analysis of the XPS spectra revealed that two intense peaks were observed at around ~863.08 and ~869.95 eV for both Ni/CeO<sub>2</sub>\_Us and Ni/CeO<sub>2</sub>\_WI catalysts. These peaks correspond to Ni 2p. The binding energy of Ni 2p is in good agreement with the binding energy reported in the literature[50, 51]. For both sonochemical and wet impregnation catalysts, only one functional group is observed in the form of Ni<sup>2+</sup>. Comparatively, the sonochemical catalyst has lower binding energy of 856 eV compared to the wet impregnation catalyst with a binding energy of 856.8 eV. This might be caused by the strong electrostatic repulsion between the functional groups and metallic ions of precursors on the surface of the support due to the introduction of ultrasound irradiation which resulted in highly intensive energy generation.

The turnover frequency (TOF), percentage dispersion and aggregate particles size were determined to evaluate the catalytic activity of Ni/CeO<sub>2</sub>\_Us and Ni/CeO<sub>2</sub>\_WI catalysts when the conversion reached 40-60% as tabulated in Table 3. The calculated TOF value of Ni/CeO<sub>2</sub>\_Us catalysts is  $2.5 \times 10^{-2} \text{ s}^{-1}$  which is higher compared to Ni/CeO<sub>2</sub>\_WI with TOF value of  $1.2 \times 10^{-2} \text{ s}^{-1}$ . This indicates that the hydrogenation rate per active sites of sonochemical catalyst is significantly higher than the wet impregnation catalyst due to larger active sites possess by sonochemical catalyst [39]. Similarly, the cumulative percentage dispersion of Ni metal was also higher for the sonochemical catalyst. The average particle size determined by TEM for Ni/CeO<sub>2</sub>\_Us and Ni/CeO<sub>2</sub>\_WI are 22 nm and 40 nm, respectively, which is in line with the average particle size determined by CO chemisorption of (18.2 nm and 36.5 nm), assuming that the particles exist in a spherical shape.

The calculated percentage dispersion of Ni/CeO<sub>2</sub>\_Us and Ni/CeO<sub>2</sub>\_WI were found to be 35.20% and 20.50%, respectively. Therefore, ultrasound irradiation has a significant effect on the particle size distribution and dispersion, TOFs, and active sites of the catalyst which enhanced the catalytic activity of the catalyst[52]. In term of the economical aspect, the combination of APR and hydrogenolysistechnology using a sonochemically synthesized catalyst is more economically feasible compared to the other conventional methods. This might be caused by the less energy consumption during the reaction which gives a significantly high yield and selectivity of 1,3-PDO within a short reaction time compared to conventional methods which operate at high reaction temperature and longer time [3, 53].

### 3.3 Optimization of reaction parameters

#### 3.3.1 Effect of glycerol to catalyst weight ratio

The experiments were performed at a reaction temperature of 230 °C with the reaction pressure of 20 bar, the reaction time of 1 h and a stirring rate of 450 rpm. The glycerol to catalyst weight ratio ( $W_{\text{glycerol}}/W_{\text{catalyst}}$ ) was varied from 3.15 to 15.77  $\text{g}_{\text{glycerol}}/\text{g}_{\text{catalyst}}$ . The data set present here are replicate of 3 data points with % error  $\pm 5$ . Fig. 10(a) shows the effect of  $W_{\text{glycerol}}/W_{\text{catalyst}}$  on the 1,3-PDO yield and selectivity and glycerol conversion. A significant increase in 1,3-PDO yield and selectivity from 3.21 to 19.54% and 4.2 to 42.73% respectively are observed when the  $W_{\text{glycerol}}/W_{\text{catalyst}}$  increased from 3.15 to 6.31  $\text{g}_{\text{glycerol}}/\text{g}_{\text{catalyst}}$ . This might be caused by the increase in the selective hydrogenolysis of glycerol to 1,3-PDO due to the increased in the amount of  $\text{H}_2$  produced via APR. The previous study conducted by Seretis and Tsiakaras [7] has reported that the production of propylene glycol via in-situ hydrogenolysis is more favoured with the increase in glycerol concentration due to the effect of an increase in autogenous pressure and maximum  $\text{H}_2$  produced at the highest glycerol concentration. Meanwhile, the 1,3-PDO yield and selectivity significantly decrease from 10.48 to 4.29% and 31.3 to 10.75% respectively with an increase in from.

The decrease in 1,3-PDO yield and selectivity at higher  $W_{\text{glycerol}}/W_{\text{catalyst}}$  above 6.31  $\text{g}_{\text{glycerol}}/\text{g}_{\text{catalyst}}$  is mainly due to the viscous glycerol solution that limits the amount of  $\text{H}_2$  dissolved in the solution and therefore reduces the availability of in-situ hydrogenolysis reaction [49]. Notably, the glycerol conversion improved significantly when the  $W_{\text{glycerol}}/W_{\text{catalyst}}$  increased from 3.15 to 9.46  $\text{g}_{\text{glycerol}}/\text{g}_{\text{catalyst}}$  and remain constant with further increased in  $W_{\text{glycerol}}/W_{\text{catalyst}}$  above 9.46  $\text{g}_{\text{glycerol}}/\text{g}_{\text{catalyst}}$  (Fig. 8). At higher  $W_{\text{glycerol}}/W_{\text{catalyst}}$ , the presence of excess reactant might cause the reaction to achieve a maximum glycerol conversion due to the

limited surface area and active sites of the catalyst present during the reaction [54]. This finding agreed with Seretis and Tsiakaras [7] reported a similar trend of increase in glycerol conversion with increased glycerol concentration. The decrease in 1,3-PDO yield and selectivity and increase in glycerol conversion at  $W_{\text{glycerol}}/W_{\text{catalyst}}$  above 6.31  $\text{g}_{\text{glycerol}}/\text{g}_{\text{catalyst}}$  might be caused by the conversion of glycerol to other side products. It has been reported in the literature that during the APR and hydrogenolysis reaction other side reaction which includes methanation reaction is simultaneously occur during this reaction which contributed to the increase in glycerol concentration [55]. Thus, from the results, it can be concluded that the optimum  $W_{\text{glycerol}}/W_{\text{catalyst}}$  is determined at 9.46  $\text{g}_{\text{glycerol}}/\text{g}_{\text{catalyst}}$ , where the maximum yield and selectivity of 1,3-PDO is obtained at this reaction condition.

### 3.3.2 Effect of temperature

The experiments were performed at a reaction pressure of 20 bar with a reaction time of 1 h, stirring rate of 450 rpm and  $W_{\text{glycerol}}/W_{\text{catalyst}}$  of 6.31  $\text{g}_{\text{glycerol}}/\text{g}_{\text{catalyst}}$ . The reaction temperature was varied from 210 to 250 °C. The data set present here are replicate of 3 data points with % error  $\pm 5$ . Fig. 10(b) shows the effect of temperature on the 1,3-PDO yield and selectivity and glycerol conversion. The results showed that the increased in temperature from 210 to 230 °C, increased the 1,3-PDO yield and selectivity from 13.2 to 19.54 % and 31.7 to 42.7% respectively. This shows that at this temperature range, this reaction is highly selective toward C-O hydrogenolysis which resulted in high yield and selectivity of 1,3-PDO. The previous study conducted by Seretis and Tsiakaras [7] has proved that the increased in temperature from 200 to 220 °C, significantly increased the  $\text{H}_2$  selectivity from 23.2 to 29.7% which resulted in a higher conversion of methanation reaction.

Meanwhile, an additional increased in temperature from 240 to 250 °C slightly reduce the 1,3-PDO yield and selectivity from 17.1 to 11.8% and 39.2 to 23.0% respectively. This might be caused by the reduction in the H<sub>2</sub> solubility in the glycerol aqueous solution at higher temperature as agreed by García, Valiente [56]. At this point, it is important to refer that, at a higher temperature, 1,3-PDO might act as a reactant that is being converted into other chemical products. As reported in the literature, 1,3-PDO is produced as an intermediate product during the hydrogenolysis of glycerol which makes it less stable and can be further converted into other final products (1-propane or propane) at higher reaction temperature [4].

Moreover, for the effect of temperature on glycerol conversion, it is observed that the glycerol conversion increase from 30 to 61% with an increased in temperature from 210 to 250 °C although the 1,3-PDO yield and selectivity decreased significantly at reaction temperature above 230 °C (Fig.10(b)). The higher glycerol conversion might be contributed by the conversion of glycerol to gases and other liquid products at higher temperature as reported in the literature [35]. García, Valiente [56] reported that at low temperature (210-230 °C), the production of liquid products meanwhile at high temperature (240-250 °C), the production of gases product is favoured. The optimized temperature is determined at 230 °C, whereby, the maximum 1,3-PDO yield and selectivity of 19.5% and 42.7% are obtained respectively.

### **3.3.3 Effect of pressure**

The experiments were performed at a reaction temperature of 230 °C for a reaction time of 1 h, stirring rate of 450 rpm and  $W_{\text{glycerol}}/W_{\text{catalyst}}$  of 6.31  $\text{g}_{\text{glycerol}}/\text{g}_{\text{catalyst}}$ . The pressure was varied from 10 to 30 bar. The data set present here are replicate of 3 data points with % error  $\pm 5$ . Fig. 10(c) shows the effect of pressure on 1,3-PDO yield and selectivity and glycerol conversion. From

the result, it is observed that the 1,3-PDO yield and selectivity increase slightly from 8.4 to 19.5% and 34.6 to 42.7% respectively with an increase in reaction pressure from 10 to 20 bar. This might be caused by the increased in the H<sub>2</sub> solubility with an increase in reaction pressure which favours hydrogenation reaction. As reported in the literature, for an aqueous phase reaction, the pressure has a significant effect on the H<sub>2</sub> solubility in the reaction system[55]. It is agreed that the increase in pressure, increase the H<sub>2</sub> solubility which improved the hydrogenolysis reaction.

The surplus increased in pressure from 25 to 30 bar, decreased the 1,3-PDO yield and selectivity from 15.9 to 7.0% and 39.9 to 30.2% respectively. This can be attributed to the conversion of 1,3-PDO to other final liquid products via hydrogenolysis reaction due to the increased in H<sub>2</sub> solubility in the reaction system with increased pressure. For the effect of pressure on glycerol conversion, it is observed that the increase in pressure from 10 to 30 bar, significantly increase the glycerol conversion from 22.9 to 56.6% (Fig. 10(c)). This result agreed with the reported literature that the increase in pressure leads to an increase in glycerol concentration as more glycerol can be converted to other liquid and gases products [55]. The optimized temperature is determined at 20 bar, whereby, at this pressure, the maximum 1,3-PDO yield and selectivity of 19.54% and 42.73% are obtained respectively.

#### **4 Conclusion**

The sonochemical method for the synthesis of mesoporous Ni- Ca/CeO<sub>2</sub> catalysts have become a new development in 1,3-PDO production via APR and selective hydrogenolysis of glycerol. The present study showed that the catalytic activity of the catalysts decreases with an increase in Ca loading. Hence, there is no significant effect of Ca loading for 1,3-PDO selectivity and yield. Whereas, Ni/CeO<sub>2</sub>\_Us catalysts showed the highest catalytic activity for APR and

selective hydrogenolysis reactions with the highest yield of 1,3-PDO(19.54%). The highest catalytic activity achieved by the sonochemically synthesizes catalyst is due to the higher surface area, smaller crystallite size and homogeneous particles distribution. This is also supported by TOF which shows that Ni/CeO<sub>2</sub>\_Us catalyst has more active sites. Therefore, it can conclude that ultrasound irradiation has a significant effect in improving the physicochemical properties as well as the catalytic activity. The distribution of the desired products is strongly dependent on the reaction conditions and catalyst preparation method. The best-designed catalysts were further utilized to optimize the reaction parameters and their effects on the 1,3-PDO yield and selectivity and glycerol conversion. The results revealed that using 6.31 g<sub>glycerol</sub>/g<sub>catalyst</sub>, at 230 °C and 20 bar produced the highest yield and selectivity of 1,3-PDO obtained i.e. (19.54%) and (42.73%) respectively. The monometallic Ni/CeO<sub>2</sub> catalysts synthesized via sonochemical method proved as a novel alternative for 1,3-PDO production through APR and selective hydrogenolysis of glycerol. In future work, a continuous reaction system could be used to investigate this similar process to improve the selectivity of 1,3-PDO and the conversion rate. Moreover, longer reaction times are expected to increase the selectivity of 1,3-PDO which simultaneously increase the contact time between reactant and catalyst.

## **Acknowledgement**

The authors would like to acknowledge the Yayasan Universiti Teknologi PETRONAS for funding this project (YUTP-015LCO-091), and Universiti Teknologi PETRONAS for the financial support and Graduate Assistant(GA) scheme. The authors also would like to thank Centralized Analytical Lab(CAL) UTP for providing analytical equipment to do the analysis

## References

1. Samudrala, S.P., S. Kandasamy, and S. Bhattacharya, Turning biodiesel waste glycerol into 1, 3-Propanediol: catalytic performance of sulphuric acid-activated montmorillonite supported platinum catalysts in glycerol hydrogenolysis. *Scientific reports*, 2018. **8**(1): p. 7484.
2. Wang, C. and C. Chen, Stabilized hydrogenolysis of glycerol to 1, 3-propanediol over Mg modified Pt/WO<sub>x</sub>-ZrO<sub>2</sub> catalysts. *Reaction Kinetics, Mechanisms and Catalysis*, 2019. **128**(1): p. 461-477.
3. Shi, G., et al., Selective hydrogenolysis of glycerol to 1,3-propanediol over Pt-WO<sub>x</sub>/SAPO-34 catalysts. *Molecular Catalysis*, 2018. **456**: p. 22-30.
4. Wei, R., et al., Hydrogenolysis of glycerol to propanediols over silicotungstic acid catalysts intercalated with CuZnFe hydrotalcite-like compounds. *Catalysis Today*, 2021.
5. Li, L.-J., et al., Hydrogenation of 3-hydroxypropanal into 1, 3-propanediol over bimetallic Ru-Ni catalyst. *RSC advances*, 2017. **7**(51): p. 32027-32037.
6. Joo, S., S. Kwak, and M.C. Lee, Effect of fuel line acoustics on the flame dynamics of H<sub>2</sub>/CH<sub>4</sub> syngas in a partially premixed gas turbine combustor. *Fuel*, 2021. **285**: p. 119231.
7. Seretis, A. and P. Tsiakaras, Crude bio-glycerol aqueous phase reforming and hydrogenolysis over commercial SiO<sub>2</sub>Al<sub>2</sub>O<sub>3</sub> nickel catalyst. *Renewable Energy*, 2016. **97**: p. 373-379.
8. Larimi, A.S., M. Kazemeini, and F. Khorasheh, Aqueous phase reforming of glycerol using highly active and stable Pt<sub>0.05</sub>Ce<sub>x</sub>Zr<sub>0.95-x</sub>O<sub>2</sub> ternary solid solution catalysts. *Applied Catalysis A: General*, 2016. **523**: p. 230-240.
9. Arandia, A., et al., Aqueous-phase reforming of bio-oil aqueous fraction over nickel-based catalysts. *International Journal of Hydrogen Energy*, 2019. **44**(26): p. 13157-13168.
10. Boga, D.A., et al., Aqueous-phase reforming of crude glycerol: effect of impurities on hydrogen production. *Catalysis Science & Technology*, 2016. **6**(1): p. 134-143.
11. Duarte, H., M. Sad, and C. Apesteguía, Aqueous phase reforming of sorbitol on Pt/Al<sub>2</sub>O<sub>3</sub>: Effect of metal loading and reaction conditions on H<sub>2</sub> productivity. *international journal of hydrogen energy*, 2016. **41**(39): p. 17290-17296.
12. Subramanian, N.D., et al., Optimised hydrogen production by aqueous phase reforming of glycerol on Pt/Al<sub>2</sub>O<sub>3</sub>. *International Journal of Hydrogen Energy*, 2016. **41**(41): p. 18441-18450.
13. Mishra, N.K., et al., Synthesis of Cu-based catalysts for hydrogenolysis of glycerol to 1,2-propanediol with in-situ generated hydrogen. *Journal of Environmental Chemical Engineering*, 2021. **9**(4): p. 105263.
14. Raso, R., et al., Aqueous phase hydrogenolysis of glycerol over Ni/Al-Fe catalysts without external hydrogen addition. *Applied Catalysis B: Environmental*, 2021. **283**: p. 119598.
15. Liu, S., et al., Hydrogenolysis of glycerol with in-situ produced H<sub>2</sub> by aqueous-phase reforming of glycerol using Pt-modified Ir-ReO<sub>x</sub>/SiO<sub>2</sub> catalyst. *Catalysis Today*, 2017.

16. Wen, Y., et al., Promoting effect of Ru in the Pt-Ru/WO<sub>x</sub>/Al<sub>2</sub>O<sub>3</sub> catalyst for the selective hydrogenolysis of glycerol to 1, 3-propanediol. *Reaction Kinetics, Mechanisms and Catalysis*, 2021. **132**(1): p. 219-233.
17. Numpilai, T., et al., Sustainable utilization of waste glycerol for 1,3-propanediol production over Pt/WO<sub>x</sub>/Al<sub>2</sub>O<sub>3</sub> catalysts: Effects of catalyst pore sizes and optimization of synthesis conditions. *Environmental Pollution*, 2021. **272**: p. 116029.
18. Sun, D., et al., Glycerol hydrogenolysis into useful C3 chemicals. *Applied Catalysis B: Environmental*, 2016. **193**: p. 75-92.
19. Zhao, X., et al., Selective Hydrogenolysis of Glycerol to 1, 3-Propanediol: Manipulating the Frustrated Lewis Pairs by Introducing Gold to Pt/WO<sub>x</sub>. *ChemSusChem*, 2017. **10**(5): p. 819-824.
20. de Andrade, T.S., M.M. Souza, and R.L. Manfro, Hydrogenolysis of glycerol to 1, 2-propanediol without external H<sub>2</sub> addition in alkaline medium using Ni-Cu catalysts supported on Y zeolite. *Renewable Energy*, 2020. **160**: p. 919-930.
21. Teo, S.H., et al., Heterogeneous calcium-based bimetallic oxide catalyzed transesterification of *Elaeis guineensis* derived triglycerides for biodiesel production. *Energy Conversion and Management*, 2017. **141**: p. 20-27.
22. Gong, H., et al., Boosting the Long-Term Stability of Hydrotalcite-Derived Catalysts in Hydrogenolysis of Glycerol by Incorporation of Ca(II). *ACS Sustainable Chemistry & Engineering*, 2021. **9**(5): p. 2246-2259.
23. Akbari, E., S.M. Alavi, and M. Rezaei, CeO<sub>2</sub> Promoted Ni-MgO-Al<sub>2</sub>O<sub>3</sub> nanocatalysts for carbon dioxide reforming of methane. *Journal of CO<sub>2</sub> Utilization*, 2018. **24**: p. 128-138.
24. Mierczynski, P., et al., High active and selective Ni/CeO<sub>2</sub>-Al<sub>2</sub>O<sub>3</sub> and Pd-Ni/CeO<sub>2</sub>-Al<sub>2</sub>O<sub>3</sub> catalysts for oxy-steam reforming of methanol. *Catalysts*, 2018. **8**(9): p. 380.
25. Bastan, F., M. Kazemeini, and A.S. Larimi, Aqueous-phase reforming of glycerol for production of alkanes over Ni/Ce<sub>x</sub>Zr<sub>1-x</sub>O<sub>2</sub> nano-catalyst: Effects of the support's composition. *Renewable Energy*, 2017. **108**: p. 417-424.
26. Amulya, M.S., et al., Sonochemical synthesis of MnFe<sub>2</sub>O<sub>4</sub> nanoparticles and their electrochemical and photocatalytic properties. *Journal of Physics and Chemistry of Solids*, 2021. **148**: p. 109661.
27. Ahmadi, F., M. Haghighi, and H. Ajamein, Sonochemically coprecipitation synthesis of CuO/ZnO/ZrO<sub>2</sub>/Al<sub>2</sub>O<sub>3</sub> nanocatalyst for fuel cell grade hydrogen production via steam methanol reforming. *Journal of Molecular Catalysis A: Chemical*, 2016. **421**: p. 196-208.
28. Ameen, M., et al., Physicochemical Properties of Ni-Mo/ $\gamma$ -Al<sub>2</sub>O<sub>3</sub> Catalysts Synthesized via Sonochemical Method. *Procedia Engineering*, 2016. **148**: p. 64-71.
29. Shan, Y.-Q., et al., Supercritical water gasification of waste water produced from hydrothermal liquefaction of microalgae over Ru catalyst for production of H<sub>2</sub> rich gas fuel. *Fuel*, 2021. **292**: p. 120288.
30. Feng, S., et al., Improving Selectivity to 1,3-Propanediol for Glycerol Hydrogenolysis Using W- and Al-Incorporated SBA-15 as Support for Pt Nanoparticles. *Industrial & Engineering Chemistry Research*, 2019. **58**(8): p. 2661-2671.
31. Xu, L., et al., CO<sub>2</sub> methanation over Ca doped ordered mesoporous Ni-Al composite oxide catalysts: The promoting effect of basic modifier. *Journal of CO<sub>2</sub> Utilization*, 2017. **21**: p. 200-210.

32. Lei, N., et al., Effective Hydrogenolysis of Glycerol to 1,3-Propanediol over Metal-Acid Concerted Pt/WO<sub>x</sub>/Al<sub>2</sub>O<sub>3</sub> Catalysts. *ChemCatChem*, 2019. **11**(16): p. 3903-3912.
33. Muhammad Azizi Topek, M.R.M.R., Mohammad Tazli Azizan, Anita Ramli, The Production of 1, 3-Propanediol Via Aqueous Phase Reforming of Sorbitol Over Sonosynthesized Ca Doped Ni/TiO<sub>2</sub>. Bachelor of Engineering(Chemical) Dissertation, 2017.
34. Liu, L., et al., Selective Hydrogenolysis of Glycerol to 1,3-Propanediol over Rhenium-Oxide-Modified Iridium Nanoparticles Coating Rutile Titania Support. *ACS Catalysis*, 2019. **9**(12): p. 10913-10930.
35. Remón, J., et al., Production of gaseous and liquid chemicals by aqueous phase reforming of crude glycerol: Influence of operating conditions on the process. *Energy Conversion and Management*, 2016. **110**: p. 90-112.
36. Chen, A., et al., Recyclable CeO<sub>2</sub>-ZrO<sub>2</sub> and CeO<sub>2</sub>-TiO<sub>2</sub> mixed oxides based Pt catalyst for aqueous-phase reforming of the low-boiling fraction of bio-oil. *International Journal of Hydrogen Energy*, 2017. **42**(15): p. 9577-9588.
37. Rajivgandhi, G.N., et al., Substantial effect of Cr doping on the antimicrobial activity of ZnO nanoparticles prepared by ultrasonication process. *Materials Science and Engineering: B*, 2021. **263**: p. 114817.
38. Rahbar Shamskar, F., F. Meshkani, and M. Rezaei, Ultrasound assisted co-precipitation synthesis and catalytic performance of mesoporous nanocrystalline NiO-Al<sub>2</sub>O<sub>3</sub> powders. *Ultrasonics Sonochemistry*, 2017. **34**: p. 436-447.
39. Ameen, M., et al., Catalytic hydrodeoxygenation of rubber seed oil over sonochemically synthesized Ni-Mo/ $\gamma$ -Al<sub>2</sub>O<sub>3</sub> catalyst for green diesel production. *Ultrasonics Sonochemistry*, 2019. **51**: p. 90-102.
40. Mulewa, W., M. Tahir, and N.A.S. Amin, MMT-supported Ni/TiO<sub>2</sub> nanocomposite for low temperature ethanol steam reforming toward hydrogen production. *Chemical Engineering Journal*, 2017. **326**: p. 956-969.
41. Zhang, L., et al., The poisoning effect of potassium ions doped on MnO<sub>x</sub>/TiO<sub>2</sub> catalysts for low-temperature selective catalytic reduction. *Applied Surface Science*, 2015. **355**: p. 1116-1122.
42. He, J., et al., Enhancement effect of oxygen mobility over Ce<sub>0.5</sub>Zr<sub>0.5</sub>O<sub>2</sub> catalysts doped by multivalent metal oxides for soot combustion. *Fuel*, 2021. **286**: p. 119359.
43. Daroughegi, R., F. Meshkani, and M. Rezaei, Enhanced activity of CO<sub>2</sub> methanation over mesoporous nanocrystalline Ni-Al<sub>2</sub>O<sub>3</sub> catalysts prepared by ultrasound-assisted co-precipitation method. *international journal of hydrogen energy*, 2017. **42**(22): p. 15115-15125.
44. Mahboob, S., M. Haghghi, and F. Rahmani, Sonochemically preparation and characterization of bimetallic Ni-Co/Al<sub>2</sub>O<sub>3</sub>-ZrO<sub>2</sub> nanocatalyst: Effects of ultrasound irradiation time and power on catalytic properties and activity in dry reforming of CH<sub>4</sub>. *Ultrasonics Sonochemistry*, 2017. **38**: p. 38-49.
45. Seretis, A. and P. Tsiakaras, Aqueous phase reforming (APR) of glycerol over platinum supported on Al<sub>2</sub>O<sub>3</sub> catalyst. *Renewable Energy*, 2016. **85**: p. 1116-1126.
46. Coronado, I., et al., Aqueous-phase reforming of methanol over nickel-based catalysts for hydrogen production. *Biomass and Bioenergy*, 2017. **106**: p. 29-37.
47. Hafizi, A., M.R. Rahimpour, and S. Hassanajili, Hydrogen production via chemical looping steam methane reforming process: Effect of cerium and calcium promoters on

- the performance of Fe<sub>2</sub>O<sub>3</sub>/Al<sub>2</sub>O<sub>3</sub> oxygen carrier. *Applied Energy*, 2016. **165**: p. 685-694.
48. García-Fernández, S., et al., The role of tungsten oxide in the selective hydrogenolysis of glycerol to 1,3-propanediol over Pt/WO<sub>x</sub>/Al<sub>2</sub>O<sub>3</sub>. *Applied Catalysis B: Environmental*, 2017. **204**: p. 260-272.
  49. Remón, J., et al., Production of gaseous and liquid chemicals by aqueous phase reforming of crude glycerol: influence of operating conditions on the process. *Energy Conversion and Management*, 2016. **110**: p. 90-112.
  50. Rivero-Mendoza, D.E., et al., An alumina-supported Ni-La-based catalyst for producing synthetic natural gas. *Catalysts*, 2016. **6**(11): p. 170.
  51. Hengne, A.M., et al., Ni-Sn-Supported ZrO<sub>2</sub> Catalysts Modified by Indium for Selective CO<sub>2</sub> Hydrogenation to Methanol. *ACS Omega*, 2018. **3**(4): p. 3688-3701.
  52. Satdeve, N.S., R.P. Ugwekar, and B.A. Bhanvase, Ultrasound assisted preparation and characterization of Ag supported on ZnO nanoparticles for visible light degradation of methylene blue dye. *Journal of Molecular Liquids*, 2019. **291**: p. 111313.
  53. Priya, S.S., et al., Platinum supported on H-mordenite: A highly efficient catalyst for selective hydrogenolysis of glycerol to 1, 3-propanediol. *ACS Sustainable Chemistry & Engineering*, 2016. **4**(3): p. 1212-1222.
  54. Vigneswaran, R., D. Balasubramanian, and B.S. Sastha, Performance, emission and combustion characteristics of unmodified diesel engine with titanium dioxide (TiO<sub>2</sub>) nano particle along with water-in-diesel emulsion fuel. *Fuel*, 2021. **285**: p. 119115.
  55. Seretis, A. and P. Tsiakaras, Hydrogenolysis of glycerol to propylene glycol by in situ produced hydrogen from aqueous phase reforming of glycerol over SiO<sub>2</sub>-Al<sub>2</sub>O<sub>3</sub> supported nickel catalyst. *Fuel Processing Technology*, 2016. **142**: p. 135-146.
  56. García, L., et al., Influence of operating variables on the aqueous-phase reforming of glycerol over a Ni/Al coprecipitated catalyst. *International Journal of Hydrogen Energy*, 2018. **43**(45): p. 20392-20407.
  57. Yang, C., et al., Understanding the promotional effect of Au on Pt/WO<sub>3</sub> in hydrogenolysis of glycerol to 1, 3-propanediol. *Chinese Journal of Catalysis*, 2018. **39**(8): p. 1366-1372.
  58. Wang, J., M. Yang, and A. Wang, Selective hydrogenolysis of glycerol to 1, 3-propanediol over Pt-W based catalysts. *Chinese Journal of Catalysis*, 2020. **41**(9): p. 1311-1319.
  59. Luo, W., et al., Alcohol-treated SiO<sub>2</sub> as the support of Ir-Re/SiO<sub>2</sub> catalysts for glycerol hydrogenolysis. *Chinese Journal of Catalysis*, 2016. **37**(11): p. 2009-2017.
  60. Pamphile-Adrián, A.J., et al., Selective hydrogenolysis of glycerol over Ir-Ni bimetallic catalysts. *Catalysis Today*, 2017. **289**: p. 302-308.

**Table 1.** Crystallite size, SSA, pore volume and pore size of the synthesized catalysts.

Catalyst	Average crystallite size (nm)			SSA (m <sup>2</sup> /g)	Pore volume (cm <sup>3</sup> /g)	Pore size (nm)
	NiO	CaO	CeO <sub>2</sub>			
CeO <sub>2</sub>	-	-	2.76	24.27	5.06	0.43
Ni/CeO <sub>2</sub> _Us	2.10	-	2.78	26.77	7.87	0.45
Ni/CeO <sub>2</sub> _WI	2.27	-	2.82	15.79	6.59	0.32
Ni-0.5Ca/CeO <sub>2</sub> _Us	2.23	2.03	2.80	26.03	6.73	0.41
Ni-0.5Ca/CeO <sub>2</sub> _WI	2.34	2.10	2.88	14.35	4.81	0.29
Ni-3Ca/CeO <sub>2</sub> _Us	2.30	2.14	2.85	25.36	5.63	0.41
Ni-3Ca/CeO <sub>2</sub> _WI	2.45	2.21	2.98	13.59	2.76	0.21
Ni-5Ca/CeO <sub>2</sub> _Us	2.44	2.27	2.97	24.55	4.59	0.39
Ni-5Ca/CeO <sub>2</sub> _WI	2.60	2.30	3.05	11.74	1.74	0.20

**Table 2.** Comparison of the present work with the available literature on 1,3-PDO production via the various catalytic process.

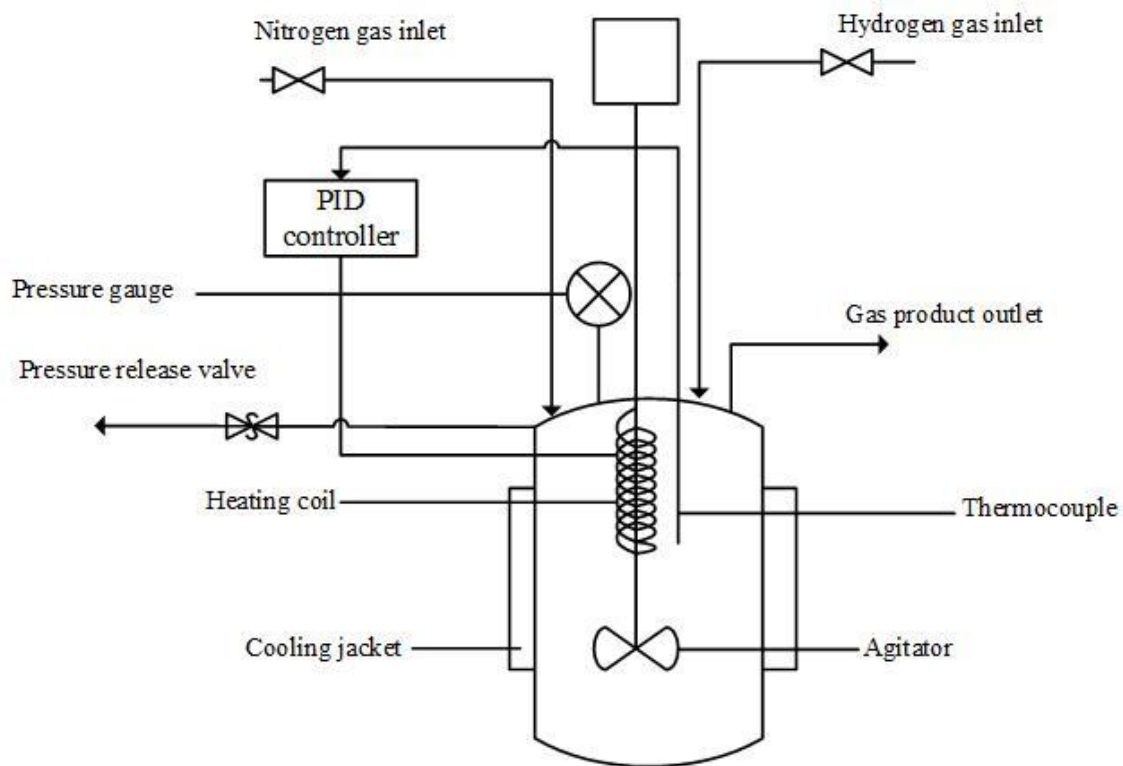
<b>Catalyst</b>	<b>Preparation method</b>	<b>Process</b>	<b>T (°C)</b>	<b>P (bar)</b>	<b>1,3-PDO Selectivity (%)</b>	<b>Glycerol conversion (%)</b>	<b>Reference</b>
Pt/WO <sub>3</sub>	SMD	Hydrogenolysis	160	10	56.93	29.71	[57]
9Pt/8W	SWI	Hydrogenolysis	200	45	51.92	53.13	[58]
Ir-Re/S-C4	CI	Hydrogenolysis	130	80	40.61	44.54	[59]
IrNi1.0	IWI	Hydrogenolysis	200	25	3.08	4.87	[60]
2Pt/S-MMT	IWI	Hydrogenolysis	200	1	62.14	94.03	[1]
Ni/CeO <sub>2</sub>	Us	APR and hydrogenolysis	230	20	42.73	54.26	This work

\*Note: SMD= Surface modified dispersion; SWI=Sequential wetness impregnation; CI= Co-impregnation; IWI=Incipient wetness impregnation; T=Temperature; P=Pressure.

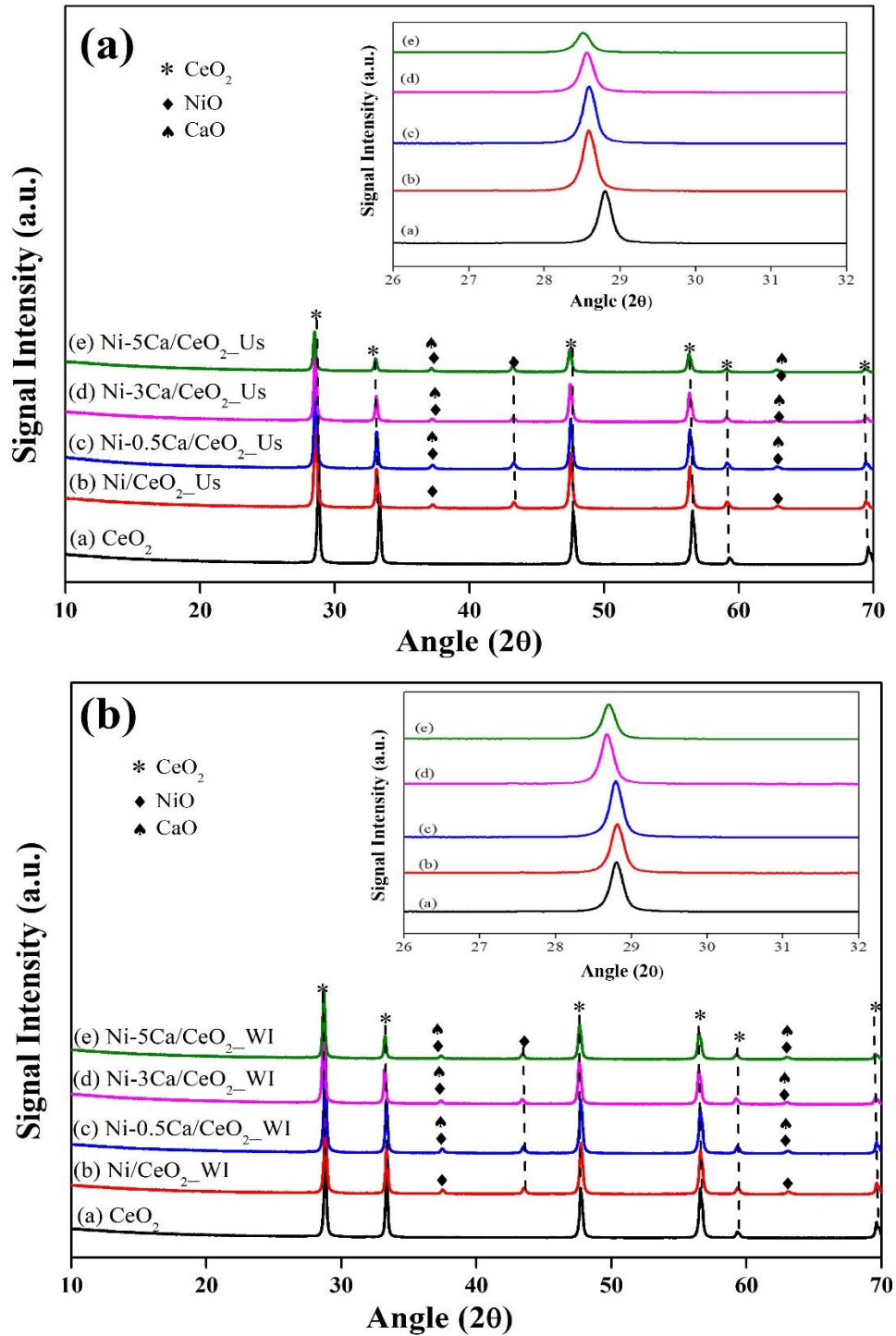
**Table 3.** TOF, percentage dispersion and particle size by CO-uptake of different catalysts; Ni/CeO<sub>2</sub>\_Us and Ni/CeO<sub>2</sub>\_WI.

<b>Catalyst</b>	<b>TOF</b> <b>(s<sup>-1</sup>)</b>	<b>Dispersion</b> <b>(%)</b>	<b>Particle size by CO-uptake</b> <b>(nm)</b>
Ni/CeO <sub>2</sub> _Us	2.5 X 10 <sup>-2</sup>	35.20	18.20
Ni/CeO <sub>2</sub> _WI	1.2 X 10 <sup>-2</sup>	20.50	36.50

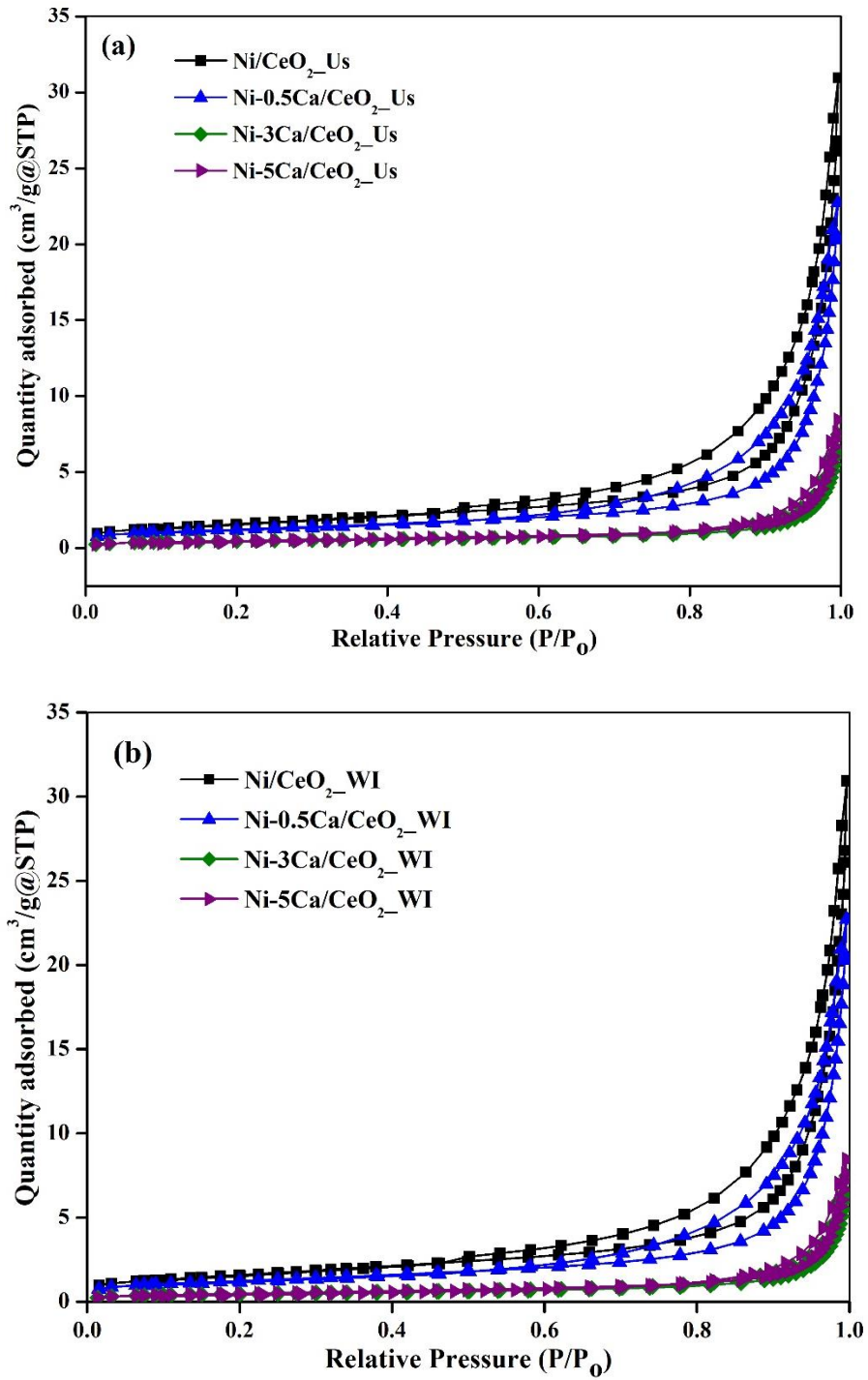
## List of Figures



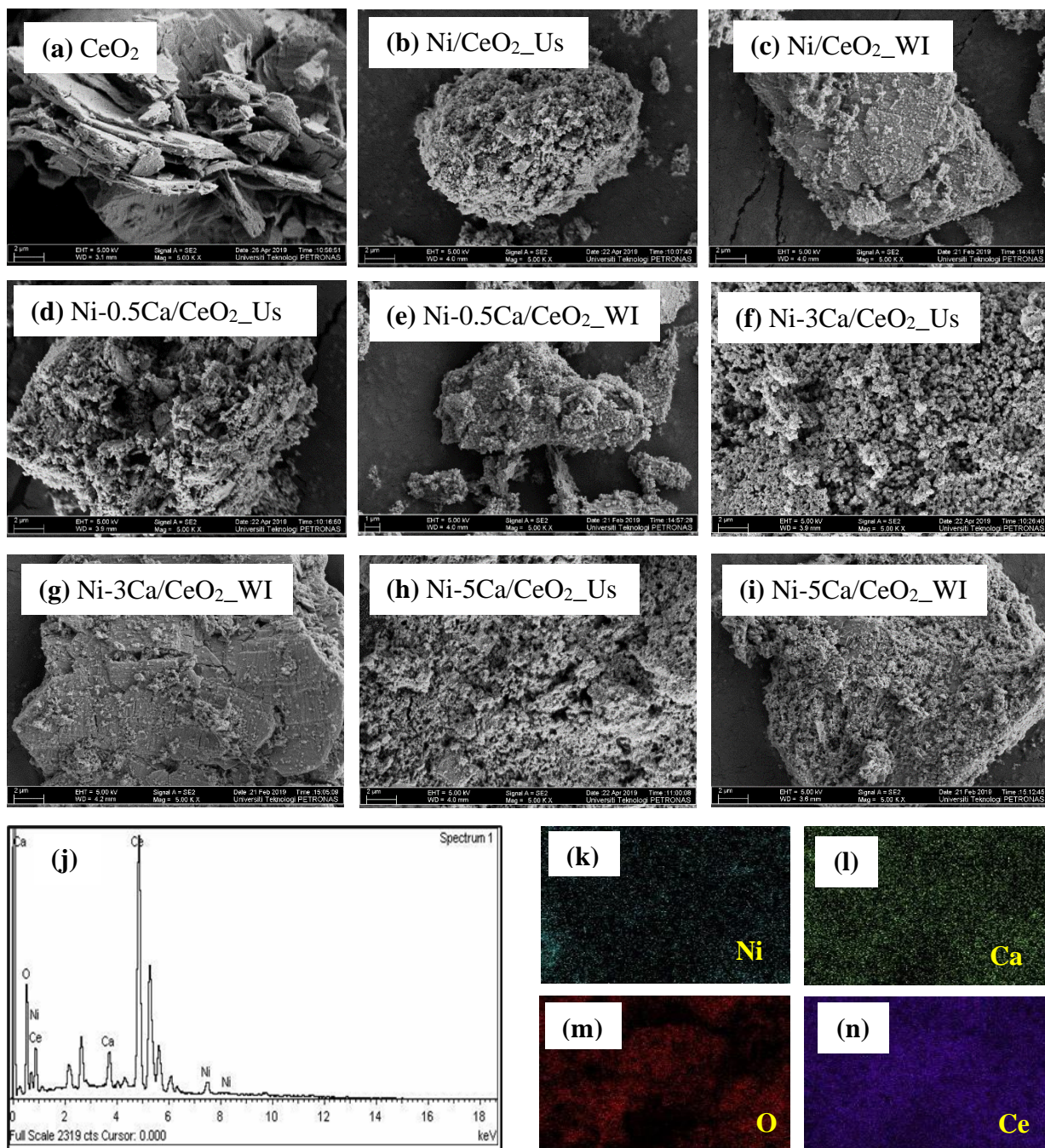
**Fig. 1.** Experimental setup for the reaction.



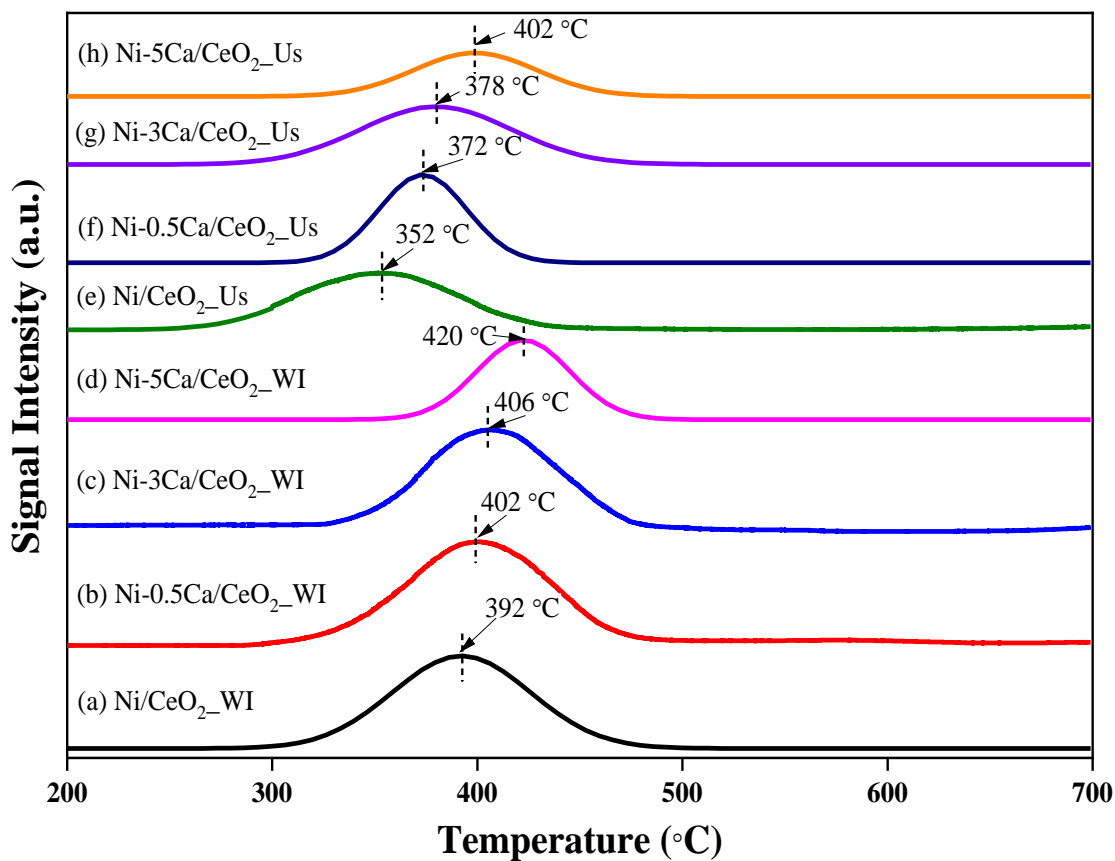
**Fig. 2.** XRD patterns of various catalysts synthesized by (a) Sonochemical and (b) Wet impregnation methods.. Inset shows the shift of the main peak with doping concentration.



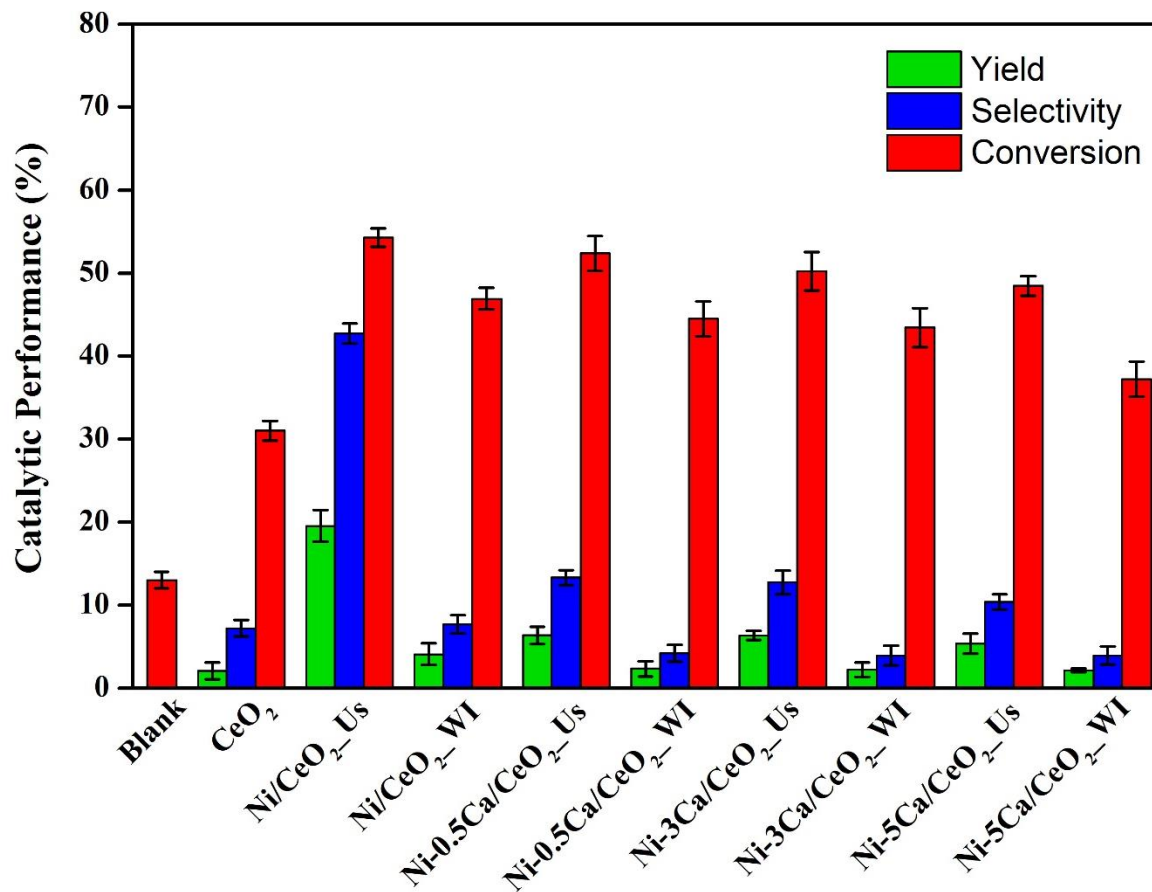
**Fig. 3.** Nitrogen adsorption-desorption isotherms of various catalysts synthesized by (a) Sonochemical and (b) Wet impregnation methods.



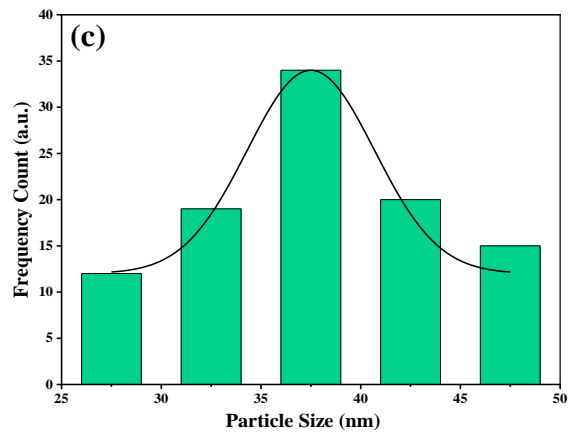
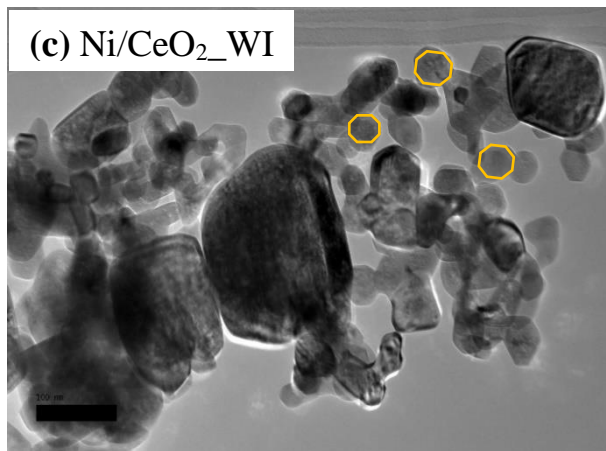
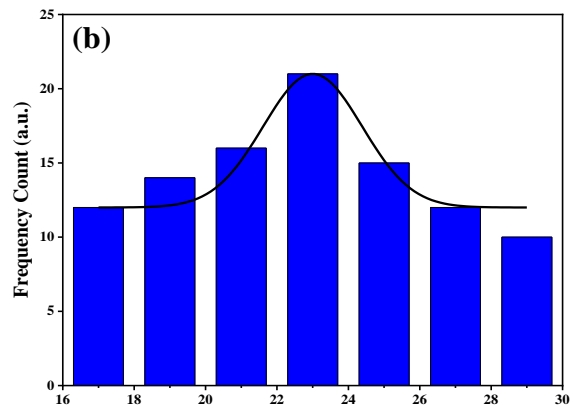
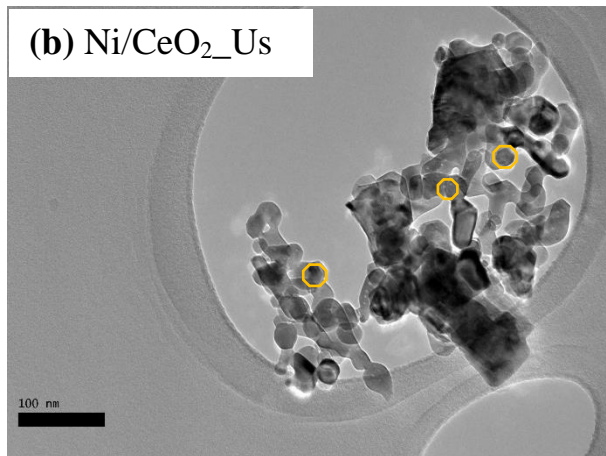
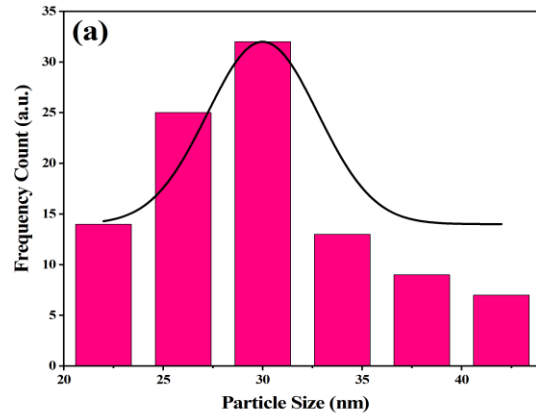
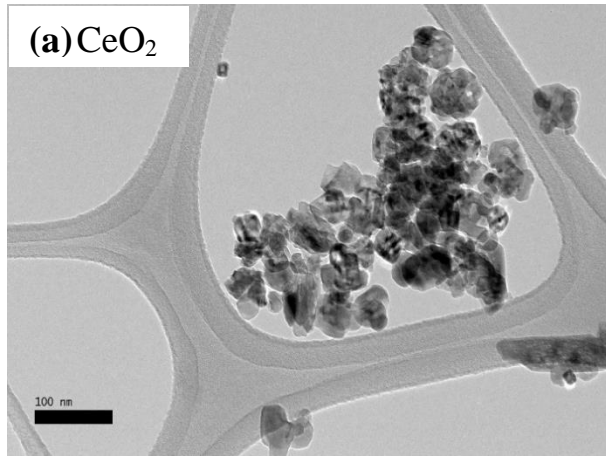
**Fig. 4.** FESEM images, EDX spectra and dot mapping images of all the synthesized catalysts.



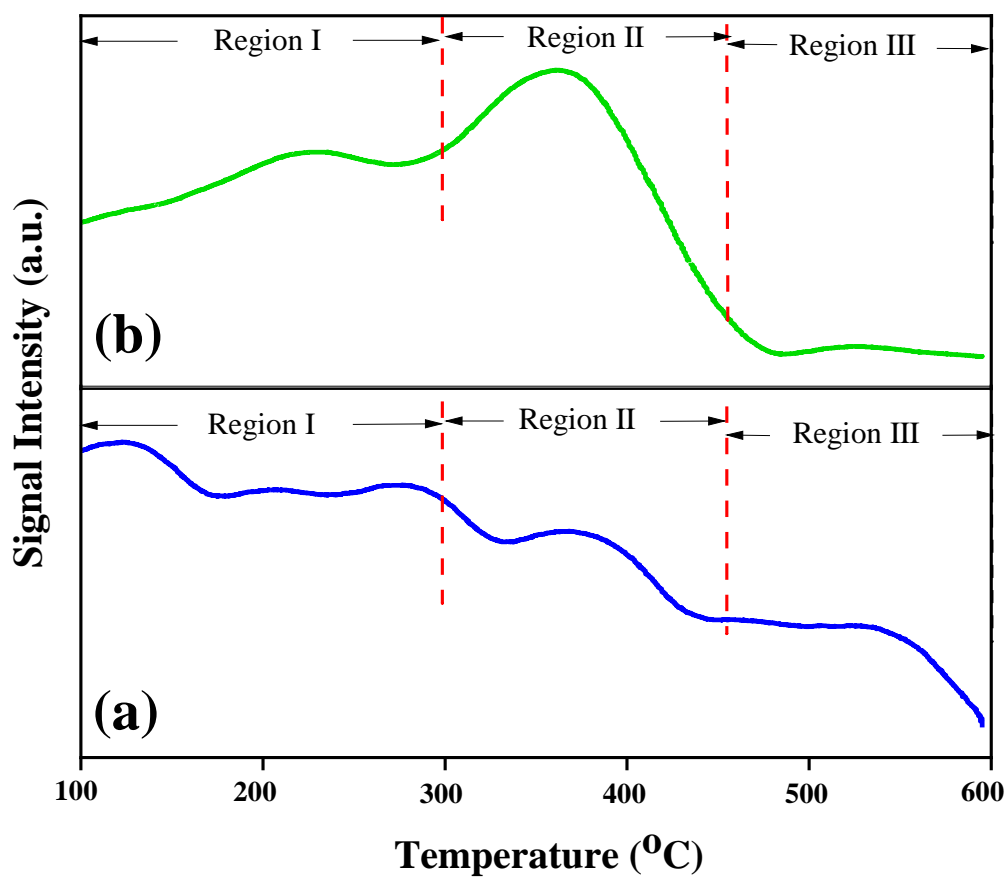
**Fig. 5.** H<sub>2</sub>-TPR profiles for various catalysts; (a) Ni/CeO<sub>2</sub>\_WI, (b) Ni-0.5Ca/CeO<sub>2</sub>\_WI, (c) Ni-3Ca/CeO<sub>2</sub>\_WI, (d) Ni-5Ca/CeO<sub>2</sub>\_WI, (e) Ni/CeO<sub>2</sub>\_Us, (f) Ni-0.5Ca/CeO<sub>2</sub>\_Us, (g) Ni-3Ca/CeO<sub>2</sub>\_Us and (h) Ni-5Ca/CeO<sub>2</sub>\_Us.



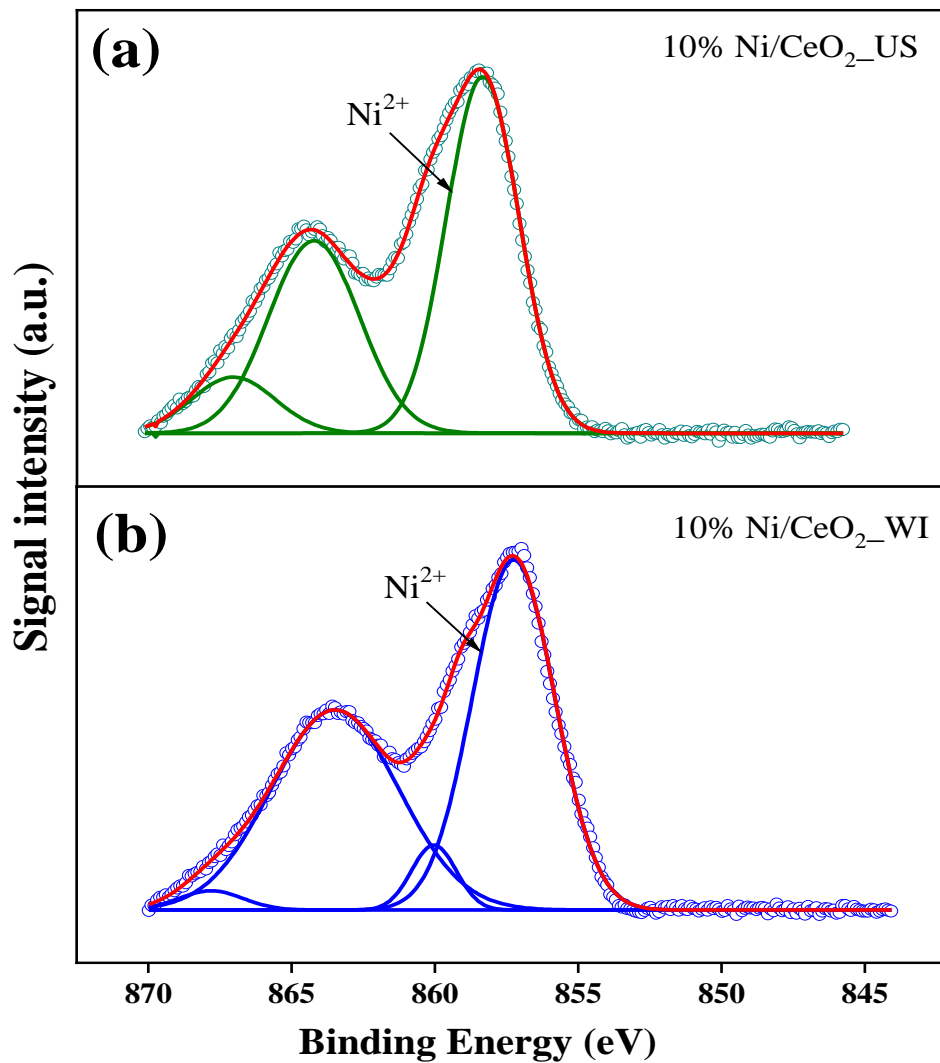
**Fig. 6.** Catalytic performance of various catalysts for APR and selective hydrogenolysis of glycerol. Reaction conditions: 10 vol.% glycerol solution, 2 g catalyst, 230 °C, 20 bar, 450 rpm and 1 h.



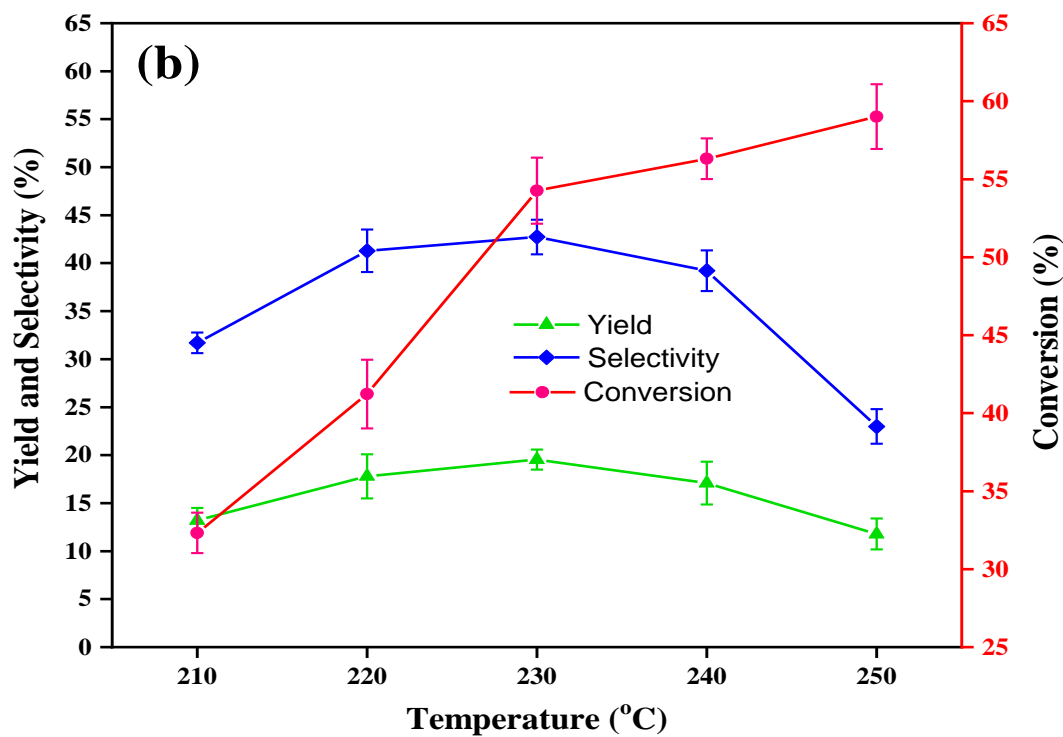
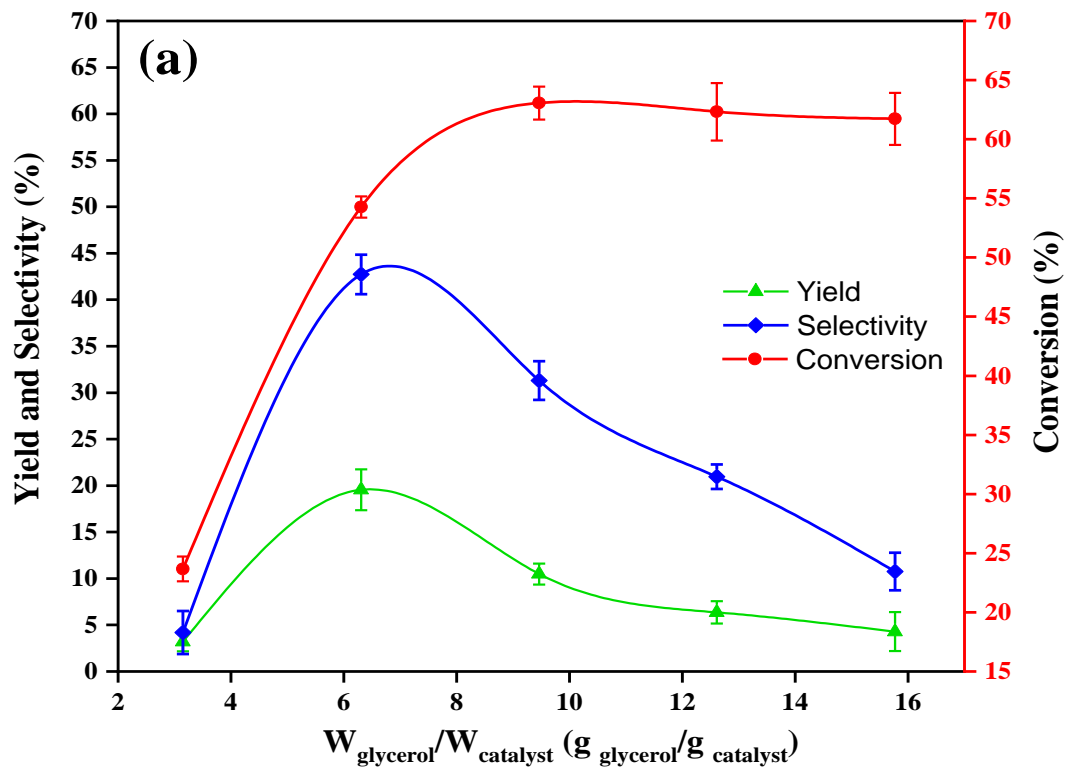
**Fig. 7.** TEM images and particle size distribution; (a) CeO<sub>2</sub>, (b) Ni/CeO<sub>2</sub>\_Us and (c) Ni/CeO<sub>2</sub>\_WI catalysts



**Fig. 8.** NH<sub>3</sub>-TPD profile for (a) Ni/CeO<sub>2</sub>\_Us and (b) Ni/CeO<sub>2</sub>\_WI catalysts.



**Fig. 9.** XPS spectra of Ni 2p for (a) Ni/CeO<sub>2</sub>-Us and (ii) Ni/CeO<sub>2</sub>-WI catalysts.



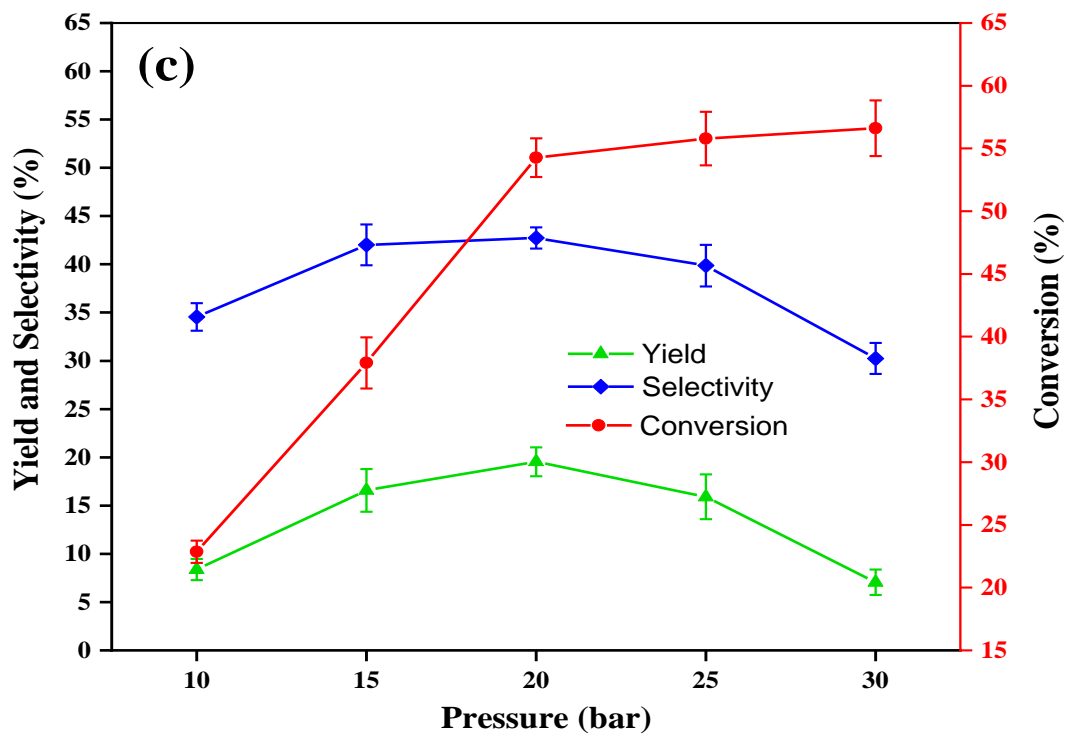


**Fig. 10.** Effect of (a)  $W_{\text{glycerol}}/W_{\text{catalyst}}$ , (b) temperature and (c) pressure on 1,3-PDO yield and selectivity and glycerol conversion.